In general, use of the same promoter may cause troubles by the homologous recombination in the simultaneous recombination. We have experienced that, when the identical promoters in the E1L and E4R sites/orientations were applied, a rearrangement through the homologous recombination occurred, whereas the AdVs in the E1L and E4L was stable. Therefore, use of different promoters would be preferable.

The harmful aberrant splicing can be avoided using the technique described herein. The aberrant splicing can be identified by PCR analysis as reported here. The preferred sequences of the splicing donor site are AGGT/AAGT (slash denotes the exon-intron junction), where the underlined GT dinucleotides are definitely required for splicing. Nucleotide mutations of these sequences, especially the GT nucleotides, can be introduced without changing the amino acid encoded by the therapeutic gene, and successful disruption of the aberrant splicing can be easily confirmed by a subsequent PCR using the same primer set. As an example, the change from T to C, G or T (Gly) in the aberrant splicing present in the TK gene removes the splicing while keeping the amino acid sequence intact, and this mutated TK gene is expected to be safer than the original TK gene for suicide gene therapy and for positron emission tomography analyses using TK gene as a reporter.

The results described here demonstrated that position effects were evident for the expression of transgenes present on the AdV genome. The mechanisms of the position effect in the AdV genome are unknown. We think that viral enhancers, silencers or other *cis*-acting sequences near to the foreign transgene promoter might influence its expression. It might be related to the fact that similar results were obtained for a strong EF1α promoter and a cancer-specific AFP promoter. In contrast to the expression levels, the vector titers were probably not influenced by the position of the transgene, because similar and high titers were obtained using a tissue-specific promoter, which does not produce the transgene mRNA in the 293 cells (Figure 2b). The results might suggest that the vector titers were mainly influenced by the combination of a strong promoter and aberrant splicing between the transgene and viral genes (Figure 2a). These results are probably valuable for efficient and safe gene therapy using FG AdVs.

In this work, the range of the E3 deletion is between two *Xba*I sites in the E3 region (nt position 28,592–30,470). Because the lengths of the E3 deletions are slightly different among the commercially available AdV construction kits, the differences might influence the results obtained here. We surmise that these differences might not influence the conclusion described here as far as the same transgene is used, because the same splicing event is essentially expected to occur by the same mechanism. However, the possibility cannot be ruled out.

The cassette plasmids (also used as cosmids) are available on request in a collaboration basis, which bear the full-length AdV genome containing the unique *Swa*I site at the E1 site and the unique *Cla*I site at the E4 site (pAxw4cit2) and that inversely containing the *Cla*I site at the E1 site and *Swa*I at the E4 site (pAxc4wit2). The method to insert a transgene into these sites is described in the Materials and Methods section.

MATERIALS AND METHODS

Cells and virus titration

Human 293,[32] HeLa and HuH-7 cell lines are derived from the human embryonic kidney, human cervical carcinoma and human hepatocellular carcinoma, respectively. The CV-1 cell line is derived from African green monkey kidney. The cells were cultured in Dulbecco's Modified Eagles Medium supplemented with 10% fetal calf serum. The 293 cells constitutively express adenoviral E1 genes and support the replication of E1-substituted AdVs. After infection with AdVs, the cells were maintained in Dulbecco's Modified Eagles Medium supplemented with 5% fetal calf serum without geneticin. FG AdVs were titrated using the method described by Pei *et al.*[16] Briefly, the copy numbers of a viral genome that was successfully transduced into the infected target cells were measured by real-time PCR (relative virus titer). HuH-7 cells were used as the target cells. The titer of the standard virus was determined using the copy number of serially diluted plasmid DNA. When FG AdVs are used, the relative virus titer (copies per ml) normally corresponds to about one-fifth of the Tissue Culture Infectious Dose 50 titer, when the gene product is not deleterious; the probable reason for this difference is that the transduction efficiency of the 293 cells is exceptionally high as compared with that of the other cells. The sequences of the TaqMan probes for the titration are derived from adenovirus-5 (Ad5) pIX gene: forward primer, 5′-TGTG ATGGGCTCCAGCATT-3′; probe, 5′-ATGGTCGCCCCGTCCTGCC-3′; reverse primer, 5′-TCGTAGGTCAAGGTAGTAGAGTTTGC-3′.

Vector construction

All the AdVs described here were constructed using the cosmid cassette pAxcwit2 containing the full-length AdV genome.[19,33] The GFP/LacZ-expression unit were under the control of the EF1α promoter[34] and the Cre-expression unit was driven by the AFP promoter; the AFP promoter used here was the (AB) 2S6 AFP promoter.[35] All the expression units were inserted into the *Swa*I cloning site at the E1 substitution region as E1L or R vectors. All the E3L and E3R vectors possessed the same expression units at the *Xba*I site in the E3 region of pAxcwit2; the *Xba*I site is originally generated by deletion between the two *Xba*I sites in the Ad5 genome (nt position 28,592-30,470). The E4 cloning site represented by the *Sna*BI site (nt position 35770) located in the E4 region at 165-nt downstream from the right end of the Ad5 genome.[17]

Conventional PCR

The PCR experiments were essentially performed by the standard method.[36] Typically, the 293 cells in the 6-well plate were infected at MOI 5 and 16 h post infection, total RNAs were prepared and reverse-transcribed using oligo(dT) primer; the resultant cDNAs were amplified by PCR with Tks Gflex DNA polymerase (Takara Bio, Shiga, Japan) and a PCR system (ProFlex PCR system, Applied Biosystems, Foster City, CA, USA). The PCR cycling conditions were in accordance with the manufacturer's protocol (Takara Bio): 94 °C for 1 min, followed by 30 cycles at 98 °C for 10 s, 60 °C for 15 s, and 68 °C for 30 s. The primer sets are described in Supplementary Table S2. The PCR products containing each splice junction were subjected to agarose gel electrophoresis.

Quantitative real-time PCR

The sequences of the GFP primers and the dsRed primers have been described previously.[17,37] The sequences of the LacZ primers were as follows: forward primer, 5′-ATCAGGATATGTGGCGGATGA-3′; probe, 5′-CGG CATTTTCCGTGACGTCT-3′; reverse primer, 5′-TGATTTGTGTAGTCGGTTTA TGCA-3′. The primer sequences of the normal splicing junctions of MLP-fiber and MLP-hexon were as follows: for MLP-fiber detection forward primer in MLP third exon, 5′-AAAGGCGTCTAACCAGTCACAGT-3′; probe in the fiber gene, 5′-AGCGCGAAGACCGTCTGAAGATACC-3′; reverse in the fiber gene, 5′-CCGCTTTCCGTGTCATATGG-3′; and for MLP-hexon detection forward primer in MLP third exon, 5′-TCTAACCAGTCACAGTCGCAAGA-3′; probe in the hexon gene, 5′-CGCGCCCGCTTTCCAAGATG-3′; reverse in the hexon gene, 5′-CACTGCGGCATCATCGAA-3′.

The mRNA levels were calculated as described by Maekawa *et al.*[37] Briefly, the total RNA of the infected cells was extracted, and the amounts of the expressed target RNAs and 18S-rRNA (correction standard) were quantified using reverse transcription (TaqMan Reverse Transcription Reagents, Roche, Basel, Switzerland) and real-time PCR (Applied Biosystems Prism 7000); the ratio of the target RNA to 18S-rRNA was then calculated. To quantify the AdV genome, the infected total cell DNA was prepared from the cells using a previously described method[29,38] or a DNA preparation kit (Macherey-Nagel, through Takara Bio). Quantitative PCR was performed to detect the AdV genome using a probe for the pIX gene, as described above.[17] The amount of chromosomal DNA was simultaneously measured to correct the Ct values of the viral genome per cell, and the corrected Ct is shown throughout. The probes were derived from the sequence of the human β-actin gene for the HeLa and HuH7 cell lines. The qPCR reaction was performed using the following cycling conditions according to the manufacturer's protocol (Applied BioSystems): 50 °C for 2 min and 95 °C for 10 min, followed by 40 cycles at 95 °C for 15 s and 60 °C for 1 min.

Measurement of the expressed GFP and LacZ

The HuH-7, HeLa and CV1 cells were infected at MOI 3 or MOI 10 of each vector in a 24-well plate in triplicated experiments. Three days after the infection, the infected cells were washed twice with phosphate-buffered saline.The cells in the three wells were then fixed with 4% paraformaldehyde to quantify the GFP fluorescence using Labsystems Fluoroskan Ascent FL (GMI, Ramsey, MN, USA) or by fluorescence microscopy. The cells infected with the LacZ vectors were harvested for the quantification of β-galactosidase (β-gal) (β-gal assay kit, Invitrogen, Carlsbad, CA, USA). To quantify the β-gal activity, the infected cells were disrupted by sonication and the lysate was subjected to a color reaction assay using o-Nitrophenyl β-D-galactopyranoside. The stained color standard was determined using 5-bromo-4-chloro-3-indolyl-β-D-galactopyranoside (X-gal).

Insertion of a transgene into the cassette plasmid (cosmid) containing both the E1 and E4 sites

The method of inserting a given transgene into the *Swa*I site of pAxw4cit2 and pAxc4wit2 is followed by the protocol of Takara Bio (Adenovirus Dual Expression Kit). Briefly, the plasmid containing the transgene DNA fragment is treated with the appropriate restriction enzymes and treated with the DNA polymerase I Klenow fragment, followed by agarose gel electrophoresis. The isolated transgene fragment of about 50 ng is ligated with 1–2 μg of the cassette cosmid at a volume of 15 μl at 15 °C for overnight. The ligated DNA is cleaved with *Swa*I to remove the self-ligated parent plasmid, and then transformation or lambda *in vitro* packaging is performed. The latter method is highly efficient and removes the deleted plasmids smaller than 38 kb. To insert a given transgene DNA to the *Cla*I site, the DNA fragment is treated with the Klenow polymerase and ligated with a DNA linker of *Bsp*T104I (Takara Bio, reaction temperature is 37 °C) or *Bst*BI (New England Biolabs, Ipswich, MA, USA, 65 °C), 5′-GGTTCGAACC-3′ (the underline shows the recognition sequences), for example, and digested with either enzyme. Because the termini produced with this enzyme can be ligated with *Cla*I-cleaved DNA and the ligated DNA cannot be cleaved with either enzyme. Therefore, after ligation of the transgene and *Cla*I-cleaved cassette, the self-ligated parent plasmid can be removed by *Cla*I digestion. Alternatively, both *Swa*I and *Cla*I sites can be converted to I-*Ceu*I, I-*Sse*I or both by insertion of the cleavage-site oligonucleotides.

CONFLICT OF INTEREST

The authors declare no conflict of interest.

ACKNOWLEDGEMENTS

We thank N Goda for research assistance and Ms T Shino for her secretarial assistance. This study was supported in part by Grants-in-Aids from the Ministry of Education, Culture, Sports, Science and Technology to YK and SK; The Program for Intractable Disease Research utilizing Disease-specific iPS Cells from JST to YK; a grant for Practical Research on Hepatitis B (009) from the Ministry of Health, Labour and Welfare of Japan to IS.

REFERENCES

1 Crystal RG. Adenovirus: the first effective in vivo gene delivery vector. *Hum Gene Ther* 2014; **25**: 3–11.
2 Watanabe M, Nasu Y, Kumon H. Adenovirus-mediated RElC/Dkk-3 gene therapy: Development of an autologous cancer vaccination therapy (Review). *Oncol Lett* 2014; **7**: 595–601.
3 Wold WS, Toth K. Adenovirus vectors for gene therapy, vaccination and cancer gene therapy. *Curr Gene Ther* 2013; **13**: 421–433.
4 Danthinne X, Imperiale MJ. Production of first generation adenovirus vectors: a review. *Gene Ther* 2000; **7**: 1707–1714.
5 Gil JS, Machado HB, Campbell DO, McCracken M, Radu C, Witte ON *et al.* Application of a rapid, simple, and accurate adenovirus-based method to compare PET reporter gene/PET reporter probe systems. *Mol Imaging Biol* 2013; **15**: 273–281.
6 Qin C, Lan X, He J, Xia X, Tian Y, Pei Z *et al.* An in vitro and in vivo evaluation of a reporter gene/probe system hERL/(18)F-FES. *PloS One* 2013; **8**: e61911.
7 Zhang G, Lan X, Yen TC, Chen Q, Pei Z, Qin C *et al.* Therapeutic gene expression in transduced mesenchymal stem cells can be monitored using a reporter gene. *Nucl Med Biol* 2012; **39**: 1243–1250.
8 Gambhir SS, Barrio JR, Phelps ME, Iyer M, Namavari M, Satyamurthy N *et al.* Imaging adenoviral-directed reporter gene expression in living animals with positron emission tomography. *Proc Natl Acad Sci USA* 1999; **96**: 2333–2338.
9 Chan HY, V S, Xing X, Kraus P, Yap SP, Ng P *et al.* Comparison of IRES and F2A-based locus-specific multicistronic expression in stable mouse lines. *Plos One* 2011; **6**: e28885.
10 Kim JH, Lee SR, Li LH, Park HJ, Park JH, Lee KY *et al.* High cleavage efficiency of a 2A peptide derived from porcine teschovirus-1 in human cell lines, zebrafish and mice. *Plos One* 2011; **6**: e18556.
11 Small JC, Kurupati RK, Zhou X, Bian A, Chi E, Li Y *et al.* Construction and characterization of E1- and E3-deleted adenovirus vectors expressing two antigens from two separate expression cassettes. *Hum Gene Ther* 2014; **25**: 328–338.
12 Pham L, Nakamura T, Gabriela Rosales A, Carlson SK, Bailey KR, Peng KW *et al.* Concordant activity of transgene expression cassettes inserted into E1, E3 and E4 cloning sites in the adenovirus genome. *J Gene Med* 2009; **11**: 197–206.
13 Yankulov K. Dynamics and stability: epigenetic conversions in position effect variegation. *Biochem Cell Biol* 2013; **91**: 6–13.
14 Wilson C, Bellen HJ, Gehring WJ. Position effects on eukaryotic gene expression. *Annu Rev Cell Biol* 1990; **6**: 679–714.
15 Nakai M, Komiya K, Murata M, Kimura T, Kanaoka M, Kanegae Y *et al.* Expression of pIX gene induced by transgene promoter: possible cause of host immune response in first-generation adenoviral vectors. *Hum Gene Ther* 2007; **18**: 925–936.
16 Pei Z, Kondo S, Kanegae Y, Saito I. Copy number of adenoviral vector genome transduced into target cells can be measured using quantitative PCR: Application to vector titration. *Biochem Biophys Res Commun* 2012; **417**: 945–950.
17 Kanegae Y, Terashima M, Kondo S, Fukuda H, Maekawa A, Pei Z *et al.* High-level expression by tissue/cancer-specific promoter with strict specificity using a single-adenoviral vector. *Nucleic Acids Res* 2011; **39**: e7.
18 Bett AJ, Haddara W, Prevec L, Graham FL. An efficient and flexible system for construction of adenovirus vectors with insertions or deletions in early regions 1 and 3. *Proc Natl Acad Sci USA* 1994; **91**: 8802–8806.
19 Miyake S, Makimura M, Kanegae Y, Harada S, Sato Y, Takamori K *et al.* Efficient generation of recombinant adenoviruses using adenovirus DNA-terminal protein complex and a cosmid bearing the full-length virus genome. *Proc Natl Acad Sci USA* 1996; **93**: 1320–1324.
20 Mizuguchi H, Kay MA. Efficient construction of a recombinant adenovirus vector by an improved in vitro ligation method. *Hum Gene Ther* 1998; **9**: 2577–2583.
21 Shin SP, Seo HH, Shin JH, Park HB, Lim DP, Eom HS *et al.* Adenovirus Expressing Both Thymidine Kinase and Soluble PD1 Enhances Antitumor Immunity by Strengthening CD8 T-cell Response. *Mol Ther* 2013; **21**: 688–695.
22 Suzuki T, Sasaki T, Yano K, Sakurai F, Kawabata K, Kondoh M *et al.* Development of a recombinant adenovirus vector production system free of replication-competent adenovirus by utilizing a packaging size limit of the viral genome. *Virus Res* 2011; **158**: 154–160.
23 Trujillo MA, Oneal MJ, McDonough S, Qin R, Morris JC. A probasin promoter, conditionallfor exampley replicating adenovirus that expresses the sodium iodide symporter (NIS) for radiovirotherapy of prostate cancer. *Gene Ther* 2010; **17**: 1325–1332.
24 Mailly L, Boulade-Ladame C, Orfanoudakis G, Deryckere F. A novel adenovirus vector for easy cloning in the E3 region downstream of the CMV promoter. *Virol J* 2008; **5**: 73.
25 Mizuguchi H, Kay MA, Hayakawa T. In vitro ligation-based cloning of foreign DNAs into the E3 and E1 deletion regions for generation of recombinant adenovirus vectors. *Biotechniques* 2001; **30**: 1112–1114; 1116.
26 Takebe Y, Seiki M, Fujisawa J, Hoy P, Yokota K, Arai K *et al.* SR alpha promoter: an efficient and versatile mammalian cDNA expression system composed of the simian virus 40 early promoter and the R-U5 segment of human T-cell leukemia virus type 1 long terminal repeat. *Mol Cellular Biol* 1988; **8**: 466–472.
27 Pei Z, Shi G, Kondo S, Ito M, Maekawa A, Suzuki M *et al.* Adenovirus vectors lacking virus-associated RNA expression enhance shRNA activity to suppress hepatitis C virus replication. *Sci Rep* 2013; **3**: 3575.
28 Mizuguchi H, Xu ZL, Sakurai F, Mayumi T, Hayakawa T. Tight positive regulation of transgene expression by a single adenovirus vector containing the rtTA and tTS expression cassettes in separate genome regions. *Hum Gene Ther* 2003; **14**: 1265–1277.
29 Saito I, Oya Y, Yamamoto K, Yuasa T, Shimojo H. Construction of nondefective adenovirus type 5 bearing a 2.8-kilobase hepatitis B virus DNA near the right end of its genome. *J Virol* 1985; **54**: 711–719.
30 Cong L, Ran FA, Cox D, Lin SL, Barretto R, Habib N *et al.* Multiplex genome engineering using CRISPR/Cas systems. *Science* 2013; **339**: 819–823.
31 Mali P, Yang LH, Esvelt KM, Aach J, Guell M, DiCarlo JE *et al.* RNA-guided human genome engineering via Cas9. *Science* 2013; **339**: 823–826.

32 Graham FL, Smiley J, Russell WC, Nairn R. Characteristics of a human cell line transformed by DNA from human adenovirus type 5. *J Gen Virol* 1977; **36**: 59–74.

33 Fukuda H, Terashima M, Koshikawa M, Kanegae Y, Saito I. Possible mechanism of adenovirus generation from a cloned viral genome tagged with nucleotides at its ends. *Microbiol Immunol* 2006; **50**: 643–654.

34 Kim DW, Uetsuki T, Kaziro Y, Yamaguchi N, Sugano S. Use of the human elongation factor-1-alpha promoter as a versatile and efficient expression system. *Gene* 1990; **91**: 217–223.

35 Sato Y, Tanaka K, Lee G, Kanegae Y, Sakai Y, Kaneko S *et al.* Enhanced and specific gene expression via tissue-specific production of Cre recombinase using adenovirus vector. *Biochem Biophys Res Commun* 1998; **244**: 455–462.

36 Sambrook J, Russell DW. *Molecular Cloning: a laboratory manual*, 3rd edn. Cold Spring Harbor Laboratory Press: Cold Spring Harbor, New York, 2001.

37 Maekawa A, Pei Z, Suzuki M, Fukuda H, Ono Y, Kondo S *et al.* Efficient production of adenovirus vector lacking genes of virus-associated RNAs that disturb cellular RNAi machinery. *Sci Rep* 2013; **3**: 1136.

38 Nakano M, Odaka K, Takahashi Y, Ishimura M, Saito I, Kanegae Y. Production of viral vectors using recombinase-mediated cassette exchange. *Nucleic Acids Res* 2005; **33**: e76.

Supplementary Information accompanies this paper on Gene Therapy website (http://www.nature.com/gt)

OPEN ACCESS Freely available online

PLOS | ONE

Adenovirus-Encoding Virus-Associated RNAs Suppress HDGF Gene Expression to Support Efficient Viral Replication

Saki Kondo[1], Kenji Yoshida[2], Mariko Suzuki[1], Izumu Saito[1], Yumi Kanegae[1]*

1 Laboratory of Molecular Genetics, Institute of Medical Science, University of Tokyo, Shirokanedai, Minato-ku, Tokyo, Japan, **2** Regenerative and Cellular Medicine Office, Sumitomo Dainippon Pharma Co., Ltd., Minatojima Minamimachi, Chuo-ku, Kobe, Japan

Abstract

Non-coding small RNAs are involved in many physiological responses including viral life cycles. Adenovirus-encoding small RNAs, known as virus-associated RNAs (VA RNAs), are transcribed throughout the replication process in the host cells, and their transcript levels depend on the copy numbers of the viral genome. Therefore, VA RNAs are abundant in infected cells after genome replication, i.e. during the late phase of viral infection. Their function during the late phase is the inhibition of interferon-inducible protein kinase R (PKR) activity to prevent antiviral responses; recently, mivaRNAs, the microRNAs processed from VA RNAs, have been reported to inhibit cellular gene expression. Although VA RNA transcription starts during the early phase, little is known about its function. The reason may be because much smaller amount of VA RNAs are transcribed during the early phase than the late phase. In this study, we applied replication-deficient adenovirus vectors (AdVs) and novel AdVs lacking VA RNA genes to analyze the expression changes in cellular genes mediated by VA RNAs using microarray analysis. AdVs are suitable to examine the function of VA RNAs during the early phase, since they constitutively express VA RNAs but do not replicate except in 293 cells. We found that the expression level of hepatoma-derived growth factor (HDGF) significantly decreased in response to the VA RNAs under replication-deficient condition, and this suppression was also observed during the early phase under replication-competent conditions. The suppression was independent of mivaRNA-induced downregulation, suggesting that the function of VA RNAs during the early phase differs from that during the late phase. Notably, overexpression of HDGF inhibited AdV growth. This is the first report to show the function, in part, of VA RNAs during the early phase that may be contribute to efficient viral growth.

Citation: Kondo S, Yoshida K, Suzuki M, Saito I, Kanegae Y (2014) Adenovirus-Encoding Virus-Associated RNAs Suppress HDGF Gene Expression to Support Efficient Viral Replication. PLoS ONE 9(10): e108627. doi:10.1371/journal.pone.0108627

Editor: Motoyuki Otsuka, The University of Tokyo, Japan

Received July 29, 2014; **Accepted** September 2, 2014; **Published** October 2, 2014

Data Availability: The authors confirm that all data underlying the findings are fully available without restriction. All relevant data except for the microarray data are within the paper and its Supporting Information files. All the data acquired by the microarray analysis were deposited in the NCBI Gene Expression Omnibus (NO. GSE58605).

Funding: This work was supported in part by Grants-in-Aid from the Ministry of Education, Culture, Sports, Science and Technology (http://www.jsps.go.jp/english/index.html) to S.K. and Y.K. and the Ministry of Health, Labour and Welfare (http://www.mhlw.go.jp/english/index.html) for Research on the Innovative Development and the Practical Application of New Drugs for Hepatitis B to I.S. This work was supported in part by the Program for Intractable Disease Research utilizing Disease-specific iPS Cells from JST to Y.K. The funders had no role in study design, data collection and analysis, decision to publish, or preparation of the manuscript.

Competing Interests: The authors of this manuscript have the following competing interests: K. Yoshida is employed by Dainippon Sumitomo Pharma Co., Ltd. This does not alter the authors' adherence to PLOS ONE policies on sharing data and materials.

* Email: kanegae@ims.u-tokyo.ac.jp

Introduction

It has become increasingly clear over the past decade that non-coding small RNAs play roles in viral life cycles at various ways [1–3]. Hepatitis C virus (HCV) is known to utilize host microRNA miR122, which is specifically expressed and highly abundant in the human liver, to support its efficient replication through its direct attachment to the HCV 5′ non-translation region; thus, miR122 is regarded as a therapeutic target for antiviral intervention [4–6]. Moreover, more than two hundred small RNAs derived from viruses have been identified. For example, Epstein-Barr virus (EBV) encodes two small RNAs, EBER-1 and EBER-2 [7–9], which modulate the interferon-mediated antiviral response [10].

Adenoviruses (Ads) encode two kinds of non-coding small-RNAs, known as virus-associated (VA) RNAs, VAI and VAII, that consist of 157–160 nucleotides (nts). After Ad infection, the transcription of VA RNAs starts at the same time as the E1A gene and lasts until the late phase. Since the transcription level of VA RNAs increases depending on the number of viral genome copies, VA RNAs in Ad-infected cells are abundant during the late phase, and this is one reason why the functional analysis of VA RNAs during the late phase has been investigated much more frequently than during the early phase.

The VA RNA I (VAI), which is expressed at a level of 10^8 copies per infected cell during the late phase [11], is required to establish efficient translation in virus-infected cells [12,13]. Moreover, it is well known that VAI inhibits anti-viral double-stranded RNA (dsRNA)-activated protein kinase (PKR). Also, VAI stabilizes ribosome-associated viral mRNAs, which could lead to enhanced levels of protein synthesis [14]. These findings have indicated that VAI plays a role in creating suitable conditions for viral growth, at

least during the late phase of infection. Recently, VA RNAs have been reported to be processed to microRNAs (mivaRNAs) via the cellular RNA-interference (RNAi) machinery, and mivaRNAs disturb cellular DNA expressions during the late phase [15]. However, it has not been investigated the function of VA RNA during the early phase, though the expression of VA RNAs starts immediately during the early phase of viral infection.

E1- and E3-deleted adenovirus vectors (AdVs), known as first-generation (FG) AdVs, have widely been used for the transient expression of transgenes in various cell types. FG AdVs lack E1A gene, an essential for viral replication; consequently, they neither express any viral gene product in target cells nor replicate except in 293 cells, which express E1A gene constitutively. However, since VA RNAs are transcribed by RNA polymerase III, their expressions are independent of E1A-mediated transactivation and they are always transcribed from AdV genome in AdV-infected cells. Therefore, FG AdVs are thought to be a suitable tool for the investigation of VA RNA function during the early phase of viral infection, since they express VA RNAs but do not replicate except in 293 cells. Moreover, these AdVs allow us to study the function of VA RNAs during both early and late phase using 293 cells. For this purpose, AdVs lacking VA RNA genes (VA-deleted AdVs) are essential as a control; however, VA-deleted AdVs have been difficult to generate and produce in quantities sufficient for practical use. Recently, we have developed a novel method for the efficient production of VA-deleted AdVs using a site-specific recombinase FLP [16]. A "pre-vector" containing the VA RNA region flanked by a pair of FRT sequences, which are target sequences for FLP recombinase, is constructed according to a commonly used method for the production of FG AdV [17]. This pre-vector, which is obtained at a high titer, is subsequently used to infect a 293 cell line that constitutively expresses humanized-FLPe [18] (293hde12) [19] so that the VA RNA region is removed from replicating viral genome. Since the excision efficiency of FLP in 293hde12 cells is high enough to remove almost all the VA RNA region from the very high number of viral genome copies, this method can be used to generate a high-titer of VA-deleted AdVs efficiently.

Here, we demonstrated the effect of VA RNAs expressed via FG AdVs on cellular gene expression by comparing the expression patterns between VA-deleted AdV- and FG AdV-infected cells using a microarray analysis. We found that VA RNAs expressed from FG AdVs disturbed the cellular gene expressions. Especially, the expression level of HDGF (hepatoma-derived growth factor; ENSG00000143321.14) was significantly decreased under the replication-deficient conditions; notably, HDGF expression started to decrease even during the early phase of infection in the 293 cells. Moreover, the overexpression of the HDGF gene inhibited viral growth in 293 cells, suggesting that the suppression of HDGF gene expression mediated by the VA RNAs was important for viral growth. This is the first report to show the function of VA RNAs during the early phase of infection.

Materials and Methods

Cells and AdVs

Human embryo kidney 293 cell line (ATCC) [20], human lung carcinoma A549 cell line (ATCC) [21], and human hepatocellular carcinoma derived HuH-7 cell line (RIKEN BRC) [22]were cultured in Dulbecco's modified Eagle's medium (DMEM) supplemented with 10% fetal calf serum (FCS). 293hde12 cell line [19], which is a 293 cell line possessing the hFLPe gene [18] (an improved version of the FLPe gene [23]), was cultured in DMEM supplemented with 10% FCS plus geneticin (0.75 mg/mL). After infection with AdVs, the cells were maintained in DMEM supplemented with 5% FCS without geneticin. For AraC (cytosine b-D-arabinofuranoside, hydrochloride: Sigma) treatment, the infected cells were maintained in DMEM supplemented with 5% FCS plus AraC (20 μg/mL).

The FG AdVs were prepared using 293 cells, which constitutively express adenoviral E1 genes and support the replication of E1-substituted AdVs. The VA-deleted AdVs except for HDGF- and GFP-expressing AdVs were prepared according to a method using 293U6VA-1 cells that constitutively express both VAI and VAII. HDGF-expressing and GFP-expressing VA-deleted AdVs were generated as described previously [16]. Briefly, an HDGF-expressing and a GFP-expressing unit under the control of the EF1α promoter was inserted into the SwaI cloning site at the authentic E1 substitution region in the pre-vector cosmid pAxdV-4FVF-w, and the pre-vectors were prepared using 293 cells. Subsequently, the pre-vectors were used to infect 293hde12 cells that constitutively express humanized FLPe recombinase [19] to excise the VA RNA region from the replicating viral genome. The VA-deleted AdVs transcribed less than 1% of the VA RNAs, compared with the FG AdVs, as confirmed using real-time PCR [16]. The VA-deleted AdVs and the FG AdVs were titrated using the methods described by Pei et al [24]. Briefly, the copy numbers of a viral genome that was successfully transduced into infected target cells were measured using qPCR (relative virus titer: rVT). This method enabled us to compare the various titers, since the transduction titer is not influenced by the growth rate of the 293 cells, even if an expressed gene product is deleterious to 293 cells.

Plasmids

The pVA41da plasmid [16] contains a DNA fragment covering all of VAI and VAII from nt position 10576–11034 of adenovirus type 5. The pBluescript SK (-) (Stratagene) was used as a control. The plasmids were transfected using Transfast (Promega). A pxEFGFP plasmid expressing GFP under the control of the EF1α promoter was used as a transfection control. Two days after the transfection of pVA41da plasmid into 293 cells, the cells were harvested and the total RNAs were extracted as described below to measure the HDGF mRNA levels using qPCR.

Microarray analysis

VA-deleted AdV (Axd12CARedE) and VA-containing FG AdV (AxCAdsRedE) were infected at an MOI (multiplicity of infection) of 0.5 to A549 cells for 24 h. We prepared triplicate samples for each of the conditions, and total RNA isolation was performed using a Qiagen RNeasy kit (Qiagen). A DNA microarray analysis using Affymetrix Gene-Chip technology was performed as described previously [25–27]. Briefly, 100 ng of total RNAs were used as a template for cDNA synthesis, and biotin-labeled cRNA was synthesized with a 3′ IVT Express Kit (Affymetrix). After generating the hybridization cocktails, hybridization to the DNA microarray (Genechip; Human Genome U133 Plus 2.0 Array; Affymetrix) [28] and fluorescent labeling were performed. The microarrays were then scanned with a GeneChip; Scanner 3000 7G System (Affymetrix). The data analysis was performed using GCOS software (Affymetrix). Signal detection and quantification were performed using the MAS5 algorithm with default settings. Global normalization was performed so that the average signal intensity of all the probe sets was equal to 100. For the clustering analysis, the signals were normalized and calculated to the individual scores, and the scores were visualized using Spotfire DecisionCite [29]. The analysis of variance among the groups was also performed using Spotfire DecisionCite and normalized data.

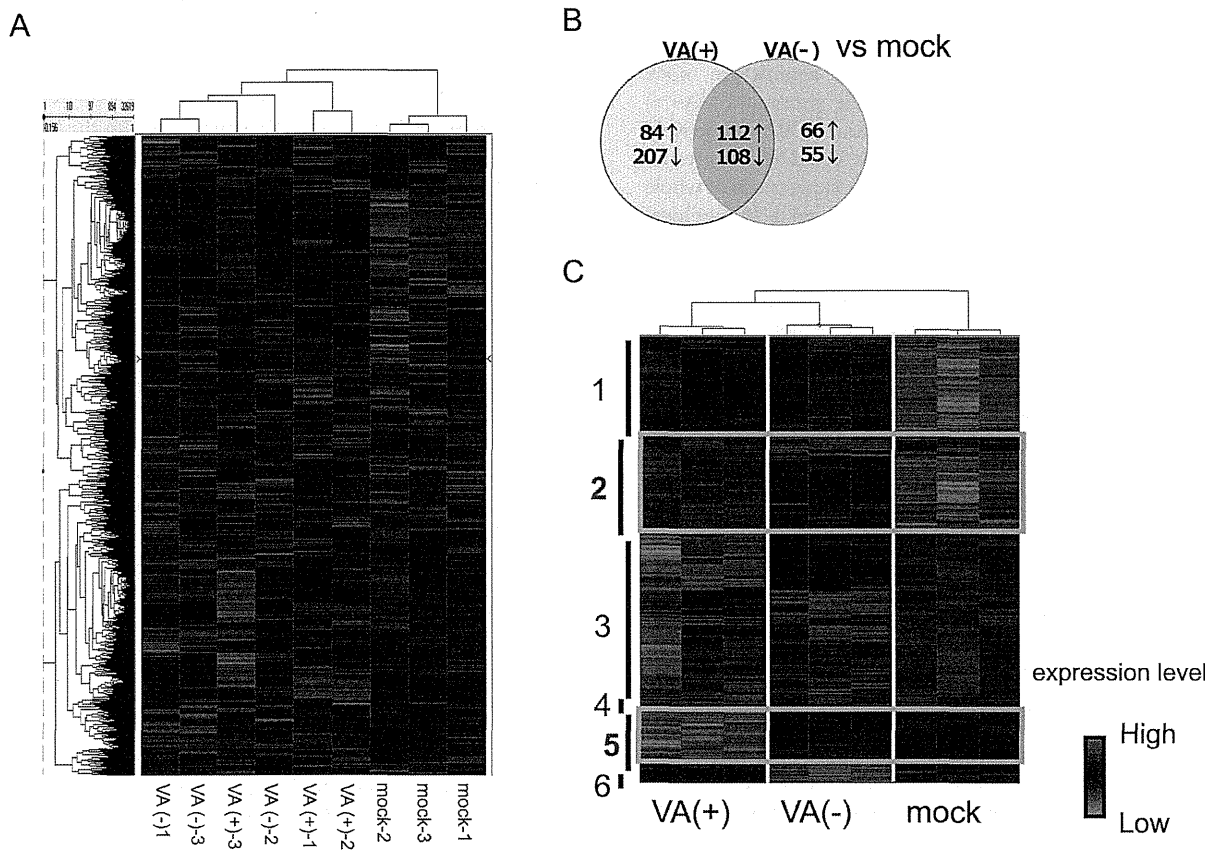

Figure 1. Microarray analysis. Global gene expression analysis of AdV infected A549 cells by Affymetrix microarray. Cells were harvested and total RNA was isolated after 24 h after infection. (A) Hierarchical clustering analysis using 32,619 genes of which expression was determined as "Present" in GCOS software in every sample. (B) The numbers of up or down regulated genes compared with mock infected group (Fold change >1.5, $P<0.01$). Red arrow indicates the numbers of up-regulated genes, and blue arrow indicates the numbers of down-regulated genes. (C) Identification and isolation of VA (+) specific gene clusters by hierarchical clustering analysis. The numbers of target genes were 2,800 genes, which were selected by ANOVA analysis in advance.
doi:10.1371/journal.pone.0108627.g001

All the data acquired by the microarray analysis were deposited in the NCBI Gene Expression Omnibus (NO. GSE58605).

Quantitative real-time PCR

The total RNA of the infected cells was extracted, and the amount of expressed target RNA and 18S-rRNA (correction standard) were quantified using reverse-transcription and real-time PCR (Applied Biosystems Villa7); the ratio of the target RNA to 18S-rRNA was then calculated. To quantify the AdV genome, the infected total cell DNA was prepared from cells using a previously described method [30,31] or a DNA preparation kit (TaKaRa Bio). Quantitative PCR (qPCR) was performed to detect the AdV genome using a probe for the pIX gene, as described previously [24]. The amount of chromosomal DNA was simultaneously measured to correct the Ct values of the viral genome per cell. The probes were derived from the sequence of the human β-actin gene for HeLa and HuH-7 cell lines. The qPCR reaction was performed according to the manufacturer's protocol: 50°C for 2 min and 95°C for 10 min, followed by 40 cycles of 95°C for 15 sec and 60°C for 1 min (Applied BioSystems).

Western blot analysis

Two days after transfection, 293 cells were harvested and the total protein was extracted using NP-40 lysis buffer [50 mM Tris-HCl (pH 8.0), 0.15M NaCl, 5 mM EDTA, 1% NP-40]. The lysates were mixed well in a rotator for 2 h at 4°C, centrifuged at 15,000 rpm for 5 min at 4°C, and the supernatants were collected. Western blotting was performed as described previously [32]. The membrane was incubated for 2 h at room temperature in the presence of anti-HDGF mouse monoclonal antibody (Bio Matrix Research, #BMR00572) diluted to 0.3 μg/mL with PBS-Tween, followed by incubation with peroxidase-conjugated goat anti-mouse IgG+IgM (Jackson Immunoresearch, #115-035-068) diluted to 1/10,000 with PBS-Tween. An anti-actin peptide goat polyclonal antibody (Santa Cruz Biotechnology, #sc-1616) diluted to 1/200 was also detected to show equal loading.

Results

HDGF gene expression was downregulated in FG-AdV infected cells

To determine whether VA RNAs expressed from FG AdVs disturb cellular gene expression, a microarray analysis was performed. We conducted a hierarchical clustering analysis using data for 32,619 genes, which were determined by GCOS software as being expressed in all the samples. The clusters were divided into two clear groups: namely, a mock group and an AdV-infected group (Figure 1A). Then, we conducted a pairwise comparison and drew a Venn diagram between the mock group vs. VA (−), i.e. VA-deleted AdV, and the mock group vs. VA (+), i.e. FG AdV,

according to the criteria of a 1.5-fold change (either an increase or a decrease) and $P<0.01$. In AdV-infected cells, more than 600 genes showed a significant increase/decrease against the mock cells in total. The numbers of VA-(+) specific genes and VA-(−) specific genes were found to be 300 and 100, respectively (Figure 1B). These results indicated that the VA RNAs expressed from AdV do not have a major impact on the expressions of whole genes. Using an ANOVA analysis ($P<0.01$) and a hierarchical clustering analysis, we isolated 6 gene clusters and 2,800 genes that showed different gene expressions between any of the group combinations. Among the 6 clusters, gene clusters 2 and 5 exhibited VA (+)-specific increases in gene expression and VA (+)-specific decreases in gene expression, respectively. According to this gene list (Table S1 in File S1) and literature survey, we finally selected several genes as targets for further research.

Next, we attempted to validate whether our microarray strategy was actually capable of identifying the targets of VA RNAs. We selected a subset of genes, all of which were upregulated or downregulated only after FG AdV infection and not after VA-deleted AdV infection, compared with the mock cells, and measured their transcript levels using quantitative RT-PCR (qPCR) in HeLa cells and HuH-7 cells. The results showed that the expression levels of some of these selected genes were actually changed in response to VA RNAs in both cell lines, except for the PTPRJ gene (Table 1). In contrast, we did not observe any significant changes in the transcript levels of TIA-1 (ENSG00000116001.11), which have been identified as a target for mivaRNA, a microRNA derived from VA RNA [15]. We chose the HDGF gene for further analysis since its transcript was remarkably decreased in both cell lines when FG AdVs were infected.

HDGF gene expression was suppressed by a lower level of VA RNAs than TIA-1

To examine whether the VA RNAs expressed from a plasmid also suppress HDGF gene expression, a VA-RNA expressing-plasmid, pVA41da [16], was transfected into 293 cells. Two days later, the total cellular RNA and protein were collected and HDGF expression was measured at the transcript level using qPCR (Figure 2A) and at the protein level using a western blot analysis (Figure 2B), respectively. The result showed that HDGF mRNA was significantly decreased, even in cells with a low level of VA-RNA transduction (Figure 2A, HDGF, 0.1 μg/well), in comparison with control plasmid-transduced cells (Figure 2A, HDGF, 0). In contrast, no significant change in TIA-1 expression was observed in the low VA RNA transduced cells (Figure 2A, TIA-1, 0.1 and 0.25), and it was suppressed only in the highest VA RNA-transduced cells (Figure 2A, TIA-1, 0.5). HDGF suppression mediated by VA RNA was also detected at the protein level (Figure 2B). The HDGF protein was significantly decreased in cells that had been transfected with the VA RNA-expressing plasmid (Figure 2B, lane 2, VA (+)), compared with the mock cells (lane 1, mock) or the control plasmid-transduced cells (lane 3, VA (−)). The suppression of HDGF transcript was also observed in VA RNA-expressing 293 cell lines named 293VA1 and 293VA42 [33], compared with that in the parent 293 cells (Table S2 in File S1). Therefore, VA RNAs suppressed HDGF expression under the conditions other than viral infection, and a smaller amount of VA RNA than TIA-1 was sufficient to suppress HDGF.

HDGF gene expression was suppressed during the early phase of viral infection

To determine the period during which HDGF was downregulated in the adenovirus life cycle, the VA-deleted AdVs and the FG-AdVs were used to infect 293 cells at an MOI of 5. Then, the cellular RNA was isolated to measure the HDGF transcript levels using qPCR at the indicated time points (Figure 3). The VA-deleted AdVs and the FG-AdVs are structurally identical except for their VA RNA expression, and these E1-deleted vectors are able to replicate in 293 cells because the E1 proteins are supplied *in trans*. The results showed that the transcript levels of HDGF started to decrease at 8 h after infection (early phase) in FG AdV-infected cells (Figure 3A, white circle). Interestingly, after VA-deleted AdV infection, the HDGF level clearly increased above the basal level at 8 h (Figure 3A, black square). This induction of HDGF expression after VA-deleted AdV infection was also observed under replication-deficient conditions in HuH-7 cells (Figure S1 in File S1, bars 1 and 3). In contrast, the TIA-1 mRNA level was similar to the basal level at 8 h and it obviously decreased to comparable level with HDGF only at 16 h (late phase) after FG-AdV infection (Figure 3B, white circle), whereas no significant upregulation was observed after VA-deleted AdV infection (Figure 3B, black square). Since the replication of the viral genome occurs at around 8 h after infection, these results showed that the suppression of HDGF and TIA-1 began during the early and late phases of viral infection, respectively. The results for TIA-1 suppression using AdVs were consistent with those of a previous report indicating that TIA-1 is downregulated during the late phase of infection with wild-type adenovirus [15]. We further examined the point that the HDGF level increased to more than 125% of the steady-state level at 8 h after VA-deleted AdV infection (Figure 3A), though the TIA-1 level did not (Figure 3B).

Table 1. Changes in expression levels of cellular genes in response to VA RNAs.

gene	ratio VA(+)/VA(−)	
	HuH-7	HeLa
PAPPA	1.23	1.60
PTPRJ	1.09	1.06
STS1-3	0.82	0.80
HDGF	0.43	0.65
TIA-1	1.10	1.09

Each mRNA level in the HuH-7 cells and HeLa cells was quantified using qPCR, and the ratio of the expression level in FG AdV infected cells (VA (+)) compared with that in VA-deleted AdV infected cells (VA (−)) was calculated.

doi:10.1371/journal.pone.0108627.t001

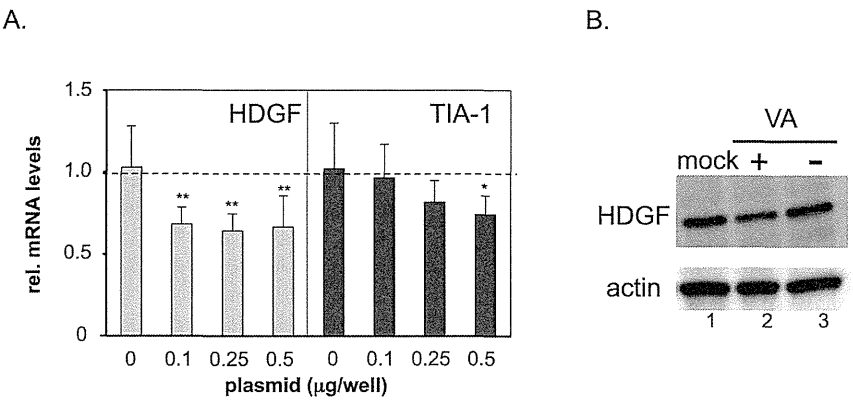

Figure 2. HDGF is downregulated in the presence of VA RNA. (A) HDGF and TIA-1 mRNA levels after VA RNA-expressing plasmid (pVAda41) transfection. RNA (A) and protein (B) were isolated after 48 h from 293 cells transfected with pVA41da or control plasmid. HDGF or TIA-1 and 18S rRNA were quantified using qPCR and plotted for comparison. The expression level in control-plasmid transfected cells was set at 1, and the ratio of the expression levels in all the cases was calculated. The error bars show the standard deviations of three different experiments. $*P<0.05$, $**P<0.01$ compared with mock cells (unpaired Student *t*-test). (B) HDGF and actin, used as a loading control, were evaluated using western blot analysis.
doi:10.1371/journal.pone.0108627.g002

VA RNAs suppressed the upregulation of HDGF gene expression during the early phase of viral infection

Although the replication of AdV genome starts 8 h after infection, the possibility that the infected cells at 8 h might contain cells reaching late phase cannot be ruled out. To examine the change in HDGF gene expression strictly during the early phase, VA-deleted and FG AdV-infected 293 cells were treated with AraC (cytosine β-D-arabinofuranosde hydrochloride), a nucleoside analog. AraC inhibits viral DNA replication and the transition from the early phase to the late phase; thus, AraC treatment amplifies the effect during the early phase. After the isolation of cellular RNA at 8 h and 24 h after infection, the transcript level of each gene was measured using qPCR and the relative mRNA level of each gene against the steady state level was calculated (Figure 4). The levels of both transcripts in AraC-treated cells at 8 h (white bars) was expected to be similar to those in untreated cells, since the replication of the viral genome had not yet started at this time point regardless of AraC treatment. Remarkably, the induction of HDGF after VA-deleted AdV infection against uninfected cells was detected at much higher levels at 24 h (bar 2) than at 8 h (bar 1). Since AraC amplifies the effect during the early phase, this result confirmed that HDGF gene expression is induced during the early phase of infection. Furthermore, after FG AdV infection with AraC treatment, no significant suppression was observed even at 24 h (bar 4), although without AraC the HDGF level was obviously decreased (Figure 3A, white circle). This result suggested that the increase in HDGF is offset by VA RNAs at 24 h in the presence of AraC, and the amount of VA RNA is not sufficient to decrease this high HDGF level below the basal level. In contrast, no significant change was observed in the TIA-1 level after VA-deleted AdV infection in AraC-treated cells (bars 5 and 6) and at 8 h after FG AdV infection (bar 7), as expected. However, the TIA-1 level was decreased at 24 h after FG AdV infection even in AraC-treated cells (bar 8), though AraC treatment inhibits transition to the late phase. The reason for this observation is unknown, but the amount of accumulated VA RNA might be sufficient for processing to mivaRNAs to suppress TIA-1 expression, which was not increased after AdV infection. Although VA RNAs suppressed both HDGF and TIA-1, the results shown here suggested that the suppression mechanism mediated by VA RNA is different from each other.

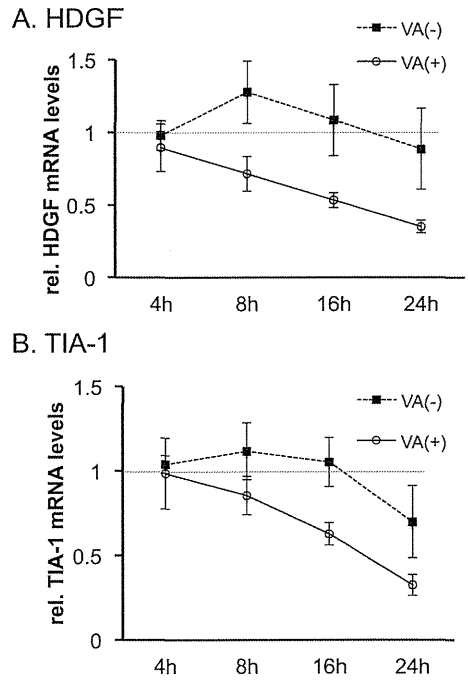

Figure 3. Suppression of HDGF begins during the early phase of viral infection. RNA was isolated from 293 cells infected with VA-deleted AdV (VA (−)) or FG AdV (VA (+)) after the indicated time periods. HDGF (A) and TIA-1 (B) mRNAs were quantified using qPCR. The expression level in uninfected cells was set at 1, and the ratio of the expression level in all the cases was calculated. The error bars show the standard deviations of three different experiments.
doi:10.1371/journal.pone.0108627.g003

Overexpression of HDGF gene inhibited VA-deleted AdV replication

Since the expression of the HDGF gene was increased after VA-deleted AdV infection during the early phase and, therefore, VA RNAs seemed to be responsible for the suppression of the increase in HDGF, we wondered whether HDGF affects viral growth. To test this hypothesis, HDGF-expressing VA-deleted AdVs and FG AdVs were constructed and used to infect 293 cells; the growth

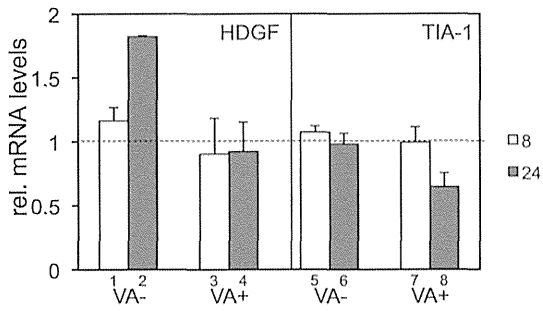

Figure 4. HDGF is upregulated during the early phase of viral infection in VA-deleted AdV-infected 293 cells. RNA was isolated from AraC-treated 293 cells infected with VA-deleted AdV (VA (−)) or FG AdV (VA (+)) after 8 h (white bars) and 24 h (gray bars), and each mRNA level was quantified using qPCR. The expression level in uninfected cells was set at 1, and the ratio of the expression level in all the cases was calculated. The error bars show the standard deviations of three different experiments.
doi:10.1371/journal.pone.0108627.g004

efficiency of each AdV was then determined using qPCR to measure the viral genome copy number (Figure 5). We applied an efficient method of generating the VA-deleted AdVs using a site-specific recombinase FLP [16]. A pre-vector, which contains VA RNA genes flanked with a pair of FRTs that are target sequences of FLP, was generated in 293 cells because it behaves as the same as FG AdVs. Subsequently, an obtained pre-vector with a high titer was used to infect 293hde12 cells [19], which are 293 cells expressing the humanized FLPe gene, to excise VA RNA genes out from the replicating AdV genome. For the efficient production of VA-deleted AdVs, a pre-vector was infected five-times more than for FG-AdV production. Under this condition, all cells are infected at once (one-step infection), and the amount of VA RNAs expressed from a pre-vector is sufficient to support the generation of HDGF-expressing VA-deleted AdVs. After AdV infection, the HDGF gene on the AdV genome is expressed exogenously under the control of a potent EF1α promoter. Therefore, the amount of HDGF protein is probably much higher than the endogenous level during AdV replication in 293 cells.

Each vector was used to infect 293 cells at an MOI of 0.5 and the infected cells were collected after 1 to 4 days. GFP-expressing AdV was used as a control. In this infection condition, only a

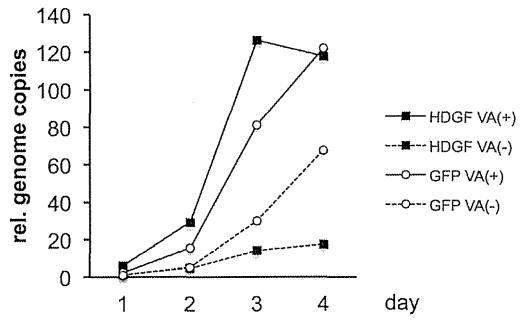

Figure 5. AdV growth in 293 cells. Total DNA was isolated from VA-deleted AdVs (VA (−)) or FG AdVs (VA (+)) infected 293 cells and each AdV genome copy was quantified using qPCR. The level of AdV genome in 293 cells after infection with GFP-expressing FG AdV on day1 was set at 1, and the ratio of the expression level in all the cases was calculated. Three independent experiments were carried out and representative results are shown.
doi:10.1371/journal.pone.0108627.g005

fraction of cells are infected and the uninfected cells are further infected by the newly produced AdVs (multistep infection). Although the growth of HDGF-expressing and GFP-expressing VA-deleted AdVs (dotted lines) was significantly lower than those of FG AdVs (solid lines), this finding was consistent with previous studies indicating a positive role of VA RNAs in viral growth [16,34]. The results clearly showed that the overexpression of the HDGF gene did not inhibit FG-AdV growth in comparison with control-FG AdV (solid lines). However, the growth of HDGF-expressing VA-deleted AdVs, the genome of which was only amplified to 20 copies on day 4, was much lower than that of GFP-expressing VA-deleted AdVs (dotted lines), which reached 70 copies. These results showed that the overexpression of the HDGF gene inhibited AdV replication as far as HDGF was not suppressed by VA RNAs.

Discussion

In this study, we demonstrated that adenovirus encoding VA RNAs suppressed HDGF gene expression. This finding revealed, for the first time, a partial role of VA RNAs in the early phase of viral infection.

The suppression of the HDGF level was observed even in cells infected with replication-deficient FG AdVs, which express a much smaller amount of VA RNAs than replicating viruses. The suppression was also detected during the early phase of viral infection in the AdV replication system, i.e., at 8 h after FG AdV infection in 293 cells. In contrast, we confirmed that TIA-1, which is suppressed by VA RNAs during the late phase of viral infection as reported by Aparicio *et al.* [15], was decreased only when VA RNAs were abundant or during the late phase of infection. Although both of these two genes, HDGF and TIA-1, were suppressed in response to VA RNAs, we revealed that the suppression of HDGF required a much smaller amount of VA RNAs than the suppression of TIA-1. This result led us to conclude that VA RNAs probably have different functions during each phase through the regulation of different gene expressions.

According to the adenovirus life cycle, the expression of E1A gene, which is a transactivator for DNA-polymerase II-dependent viral early-gene expression, starts in the immediately during the early phase. The transcription of VA RNAs mediated by DNA polymerase III is independent of E1A-regulated transcription and, therefore, starts almost at the same time as E1A. The amount of VA RNAs during the early phase is much lower than that during the late phase, since it depends on the number of genome copies, which increases to 100,000 copies per cell in the late phase. Actually, the level of VA RNAs during the early phase was about 200-times lower than that during the late phase (Table S3 in File S1). Therefore, the amount of VA RNAs expressed from replication-deficient FG-AdVs is also much smaller than that during the late phase of viral infection. It has been reported that VA RNAs are processed to microRNAs (mivaRNAs) through cellular RNAi machinery and that knockdown of Dicer using siRNA promotes the growth of VA-deleted adenoviruses [35]. However, mivaRNAs suppress TIA-1 expression only during the late phase [15] and have never been detected during the early phase of viral infection [34,36]. These findings strongly suggest that VA RNAs are processed to microRNAs only when the VA RNAs are abundant. Therefore, the suppression of HDGF gene expression by VA RNAs may not due to mivaRNAs.

In fact, our reporter assay using luciferase suggested that HDGF may not a target for mivaRNAs (Figure S2 in File S1). There is a putative target sequence for a mivaRNA in the 3′ UTR region of the HDGF gene, and we examined whether it is a target sequence

or not. As a result, no significant reduction in luciferase activity was detected when the putative seed sequence was cloned into the downstream of luciferase gene. The result suggested that, at least, the known mivaRNAs are not responsible for HDGF suppression. Together with the results shown in Figure 2 and 4, this finding indicated that the role of VA RNAs during the early phase differs from that during the late phase of viral infection, although further investigation is required to reveal the HDGF suppression mechanism mediated by VA RNAs.

The fact that the amount of VA RNA required for HDGF suppression differs from that required for TIA-1 suppression may explain why our microarray analysis did not detect the TIA-1 gene as a positive target. Aparicio *et al.* used cells transfected with a VA RNA-expressing plasmid for their microarray analysis [15]; however, it is difficult to introduce the same number of plasmid copies into 100% of the cells uniformly. Therefore, the results for cells with a high-copy number of plasmids, rather than those for cells with a low-copy number of plasmids, might be favored if a cell mixture containing both high-copy and low-copy number of plasmids is used for the microarray analysis. Consequently, they identified TIA-1 as a target of mivaRNA. In contrast, our microarray using AdVs for VA RNA transduction enabled us to introduce a small amount of VA RNAs into all the cells present in the dish in a uniform manner [18], allowing us to identify novel target genes of VA RNAs during the early phase of infection.

The E1A gene is essential for the adenovirus life cycle and viruses cannot replicate without E1A, such as AdV, which lacks the E1 genes and replicates only in E1-expressing 293 cells. Recently, the interaction of E1A with a cellular factor, CtBP (transcriptional corepressor C-terminal binding protein), has been reported to be required for the efficient E1A-mediated transactivation of early genes [37]. CtBP was initially discovered during screening for cellular factors binding to, and modulating the activity of E1A protein in Ras-mediated tumorigenesis [38]. CtBP was subsequently shown to play an important role in the regulation of cellular genes involved in growth and differentiation [39]. The C-terminal region of E1A interacts with CtBP, and an adenovirus containing the E1A mutation within the CtBP-binding motif, PLDLS, has been shown to decrease the level of early gene expression and, consequently, to inhibit viral growth.

HDGF has also been reported to be a CtBP-binding protein. Yang and Everett showed that HDGF functions as a transcriptional repressor of the SET and MYND domain containing 1 (SMYD1) gene through its interaction with CtBP using the same binding site as E1A [40]. HDGF is a transcription factor consisting of a nuclear protein with both mitogenic and angiogenic activity that is highly expressed in the developing heart and vasculature. HDGF contains an N-terminal PWWP domain and a C-terminal NLS signal. HDGF interacts with CtBP through a non-canonical binding motif (PKDLF), which is located within the PWWP domain, and represses target gene expression by binding to the promoter region leading to cell proliferation. Since both the HDGF and E1A proteins utilize the same binding site on the N-terminus of CtBP using PXDLS-like motifs [40,41], HDGF might compete with E1A to interact with CtBP. In other words, adenovirus may suppress the expression of HDGF, a cellular-CtBP binding protein, using VA RNAs so that E1A acquires an advantage for CtBP binding.

Our results showed that the upregulation of HDGF, compared with the steady-state level, was observed after infection with VA-deleted AdVs both during the early phase of the replicating condition and during replication-deficient conditions. Of note, some of other CtBP-binding proteins were also transcriptionally upregulated under the same conditions resulting in HDGF upregulation, and VA RNA suppressed these gene expressions, although the expression changes in these genes were not as noticeable as that of HDGF (Table S4 in File S1). These findings suggest that VA RNAs selectively suppress the induction in gene expressions, resulting in the expression of CtBP-binding proteins that may play a role in competitive inhibition with the E1A-CtBP interaction. Moreover, VA RNAs suppress the expression of these genes before the replication of the viral genome, i.e., during the early phase, because E1A-CtBP functions during this phase [37]. In other words, VA RNAs may act to prevent one of the host-defense mechanisms that lead to the inhibition of E1A function, which is essential for the initiation of viral replication.

In the case of AdV infection at a low MOI, which is similar to the condition for native viral infection, the growth of HDGF-expressing VA-deleted AdVs was much lower than that for GFP-expressing VA-deleted AdVs as well as FG AdVs (Figure 5). This result indicates that HDGF expression inhibits viral growth only when the replication starts from a small amount of virus. Our study using AdV at a low MOI may reflect actual viral infection during the very early phase, since a target cell does not express E1A protein before infection and viral infection does not occur at a high MOI. From this point of view, the suppression of the expression of CtBP-binding proteins mediated by VA RNAs might be advantageous for viral growth.

The E1- and E3-deleted AdVs used in this study are widely applied for various studies including gene therapy. However, this vector has two concerns. One is that it, in fact, expresses viral genes, pIX and VA RNAs. It is known that AdVs cause severe immune responses, and we have reported that a main cause is aberrant expression of immunogenic, viral pIX protein, and the pIX protein is not produced when EF1α promoter is used for transgene expression [42]. In terms of VA RNAs, it has not been clear whether a small amount of VA RNAs transcribed via AdVs affects physiological responses in the infected cells or not. The study described here is the first report to show that the VA RNAs expressed from AdVs disturb cellular gene expressions including a transcription factor, HDGF. Our results strongly suggest that production of VA RNAs would be avoided, if possible, when AdVs are applied for gene therapy, since VA RNAs expressed from FG AdVs may affect various cellular signaling pathways. Disturbance of cellular gene expression caused by VA RNAs might also affect the data in the basic study using AdVs. Moreover, although AdVs are often applied for shRNA expression, VA RNA expressed from AdVs inhibits shRNA activity [33], since VA RNAs utilize cellular RNAi machinery for processing of mivaRNAs. The present study provided further evidence that VA-deleted AdVs are useful and might be substituted for FG AdVs.

Supporting Information

File S1 **Figure S1**, HDGF is suppressed after FG AdV infection in HuH-7 cells. **Figure S2**, HDGF mRNA is not a direct target of mivaRNAI-138. **Table S1**, Gene list for gene clusters 2 and 5. **Table S2**, HDGF and TIA-1 expression levels in 293 cell lines. **Table S3**, Amount of VA RNAs after FG AdV infection in 293 cells. **Table S4**, Ratio of expression levels of genes known to be CtBP-binding proteins after AdV infection in HuH-7 cells.
(PPT)

Acknowledgments

We thank Ms. T. Shiino for her secretarial assistance and A. Maekawa and M. Yamasaki for critical readings of our manuscript, and Dr. Hiroyuki Nakagawa for assistance of microarray analysis.

Author Contributions

Conceived and designed the experiments: SK YK IS. Performed the experiments: SK KY MS. Analyzed the data: SK KY. Contributed reagents/materials/analysis tools: SK YK. Wrote the paper: SK YK IS.

References

1. Grundhoff A, Sullivan CS (2011) Virus-encoded microRNAs. Virology 411: 325–343.
2. Zhou R, Rana TM (2013) RNA-based mechanisms regulating host-virus interactions. Immunol Rev 253: 97–111.
3. Narayanan A, Kehn-Hall K, Bailey C, Kashanchi F (2011) Analysis of the roles of HIV-derived microRNAs. Expert Opin Biol Ther 11: 17–29.
4. Pedersen IM, Cheng G, Wieland S, Volinia S, Croce CM, et al. (2007) Interferon modulation of cellular microRNAs as an antiviral mechanism. Nature 449: 919–922.
5. Jopling CL, Yi M, Lancaster AM, Lemon SM, Sarnow P (2005) Modulation of hepatitis C virus RNA abundance by a liver-specific MicroRNA. Science 309: 1577–1581.
6. Fukuhara T, Matsuura Y (2013) Role of miR-122 and lipid metabolism in HCV infection. J Gastroenterol 48: 169–176.
7. Bornkamm GW (2009) Epstein-Barr virus and its role in the pathogenesis of Burkitt's lymphoma: an unresolved issue. Semin Cancer Biol 19: 351–365.
8. Lerner MR, Andrews NC, Miller G, Steitz JA (1981) Two small RNAs encoded by Epstein-Barr virus and complexed with protein are precipitated by antibodies from patients with systemic lupus erythematosus. Proc Natl Acad Sci U S A 78: 805–809.
9. Yajima M, Kanda T, Takada K (2005) Critical role of Epstein-Barr Virus (EBV)-encoded RNA in efficient EBV-induced B-lymphocyte growth transformation. J Virol 79: 4298–4307.
10. Greifenegger N, Jager M, Kunz-Schughart LA, Wolf H, Schwarzmann F (1998) Epstein-Barr virus small RNA (EBER) genes: differential regulation during lytic viral replication. J Virol 72: 9323–9328.
11. Mathews MB (1995) Structure, function, and evolution of adenovirus virus-associated RNAs. Curr Top Microbiol Immunol 199 (Pt 2): 173–187.
12. Schneider RJ, Weinberger C, Shenk T (1984) Adenovirus VAI RNA facilitates the initiation of translation in virus-infected cells. Cell 37: 291–298.
13. Reichel PA, Merrick WC, Siekierka J, Mathews MB (1985) Regulation of a protein synthesis initiation factor by adenovirus virus-associated RNA. Nature 313: 196–200.
14. O'Malley RP, Duncan RF, Hershey JW, Mathews MB (1989) Modification of protein synthesis initiation factors and the shut-off of host protein synthesis in adenovirus-infected cells. Virology 168: 112–118.
15. Aparicio O, Carnero E, Abad X, Razquin N, Guruceaga E, et al. (2010) Adenovirus VA RNA-derived miRNAs target cellular genes involved in cell growth, gene expression and DNA repair. Nucleic Acids Res 38: 750–763.
16. Maekawa A, Pei Z, Suzuki M, Fukuda H, Ono Y, et al. (2013) Efficient production of adenovirus vector lacking genes of virus-associated RNAs that disturb cellular RNAi machinery. Sci Rep 3: 1136.
17. Fukuda H, Terashima M, Koshikawa M, Kanegae Y, Saito I (2006) Possible mechanism of adenovirus generation from a cloned viral genome tagged with nucleotides at its ends. Microbiol Immunol 50: 643–654.
18. Kondo S, Takata Y, Nakano M, Saito I, Kanegae Y (2009) Activities of various FLP recombinases expressed by adenovirus vectors in mammalian cells. J Mol Biol 390: 221–230.
19. Takata Y, Kondo S, Goda N, Kanegae Y, Saito I (2011) Comparison of efficiency between FLPe and Cre for recombinase-mediated cassette exchange in vitro and in adenovirus vector production. Genes Cells 16: 765–777.
20. Graham FL, Smiley J, Russell WC, Nairn R (1977) Characteristics of a human cell line transformed by DNA from human adenovirus type 5. J Gen Virol 36: 59–74.
21. Giard DJ, Aaronson SA, Todaro GJ, Arnstein P, Kersey JH, et al. (1973) In vitro cultivation of human tumors: establishment of cell lines derived from a series of solid tumors. J Natl Cancer Inst 51: 1417–1423.
22. Nakabayashi H, Taketa K, Miyano K, Yamane T, Sato J (1982) Growth of human hepatoma cells lines with differentiated functions in chemically defined medium. Cancer Res 42: 3858–3863.
23. Buchholz F, Angrand PO, Stewart AF (1998) Improved properties of FLP recombinase evolved by cycling mutagenesis. Nat Biotechnol 16: 657–662.
24. Pei Z, Kondo S, Kanegae Y, Saito I (2012) Copy number of adenoviral vector genome transduced into target cells can be measured using quantitative PCR: application to vector titration. Biochem Biophys Res Commun 417: 945–950.
25. Heishi M, Ichihara J, Teramoto R, Itakura Y, Hayashi K, et al. (2006) Global gene expression analysis in liver of obese diabetic db/db mice treated with metformin. Diabetologia 49: 1647–1655.
26. Matsui T, Takano M, Yoshida K, Ono S, Fujisaki C, et al. (2012) Neural stem cells directly differentiated from partially reprogrammed fibroblasts rapidly acquire gliogenic competency. Stem Cells 30: 1109–1119.
27. Ishida N, Hayashi K, Hoshijima M, Ogawa T, Koga S, et al. (2002) Large scale gene expression analysis of osteoclastogenesis in vitro and elucidation of NFAT2 as a key regulator. J Biol Chem 277: 41147–41156.
28. Lockhart DJ, Dong H, Byrne MC, Follettie MT, Gallo MV, et al. (1996) Expression monitoring by hybridization to high-density oligonucleotide arrays. Nat Biotechnol 14: 1675–1680.
29. Kaushal D, Naeve CW (2004) Analyzing and visualizing expression data with Spotfire. Curr Protoc Bioinformatics Chapter 7: Unit 7 9.
30. Saito I, Groves R, Giulotto E, Rolfe M, Stark GR (1989) Evolution and stability of chromosomal DNA coamplified with the CAD gene. Mol Cell Biol 9: 2445–2452.
31. Nakano M, Odaka K, Takahashi Y, Ishimura M, Saito I, et al. (2005) Production of viral vectors using recombinase-mediated cassette exchange. Nucleic Acids Res 33: e76.
32. Baba Y, Nakano M, Yamada Y, Saito I, Kanegae Y (2005) Practical range of effective dose for Cre recombinase-expressing recombinant adenovirus without cell toxicity in mammalian cells. Microbiol Immunol 49: 559–570.
33. Pei Z, Shi G, Kondo S, Ito M, Maekawa A, et al. (2013) Adenovirus vectors lacking virus-associated RNA expression enhance shRNA activity to suppress hepatitis C virus replication. Sci Rep 3: 3575.
34. Aparicio O, Razquin N, Zaratiegui M, Narvaiza I, Fortes P (2006) Adenovirus virus-associated RNA is processed to functional interfering RNAs involved in virus production. J Virol 80: 1376–1384.
35. Bennasser Y, Chable-Bessia C, Triboulet R, Gibbings D, Gwizdek C, et al. (2011) Competition for XPO5 binding between Dicer mRNA, pre-miRNA and viral RNA regulates human Dicer levels. Nat Struct Mol Biol 18: 323–327.
36. Andersson MG, Haasnoot PC, Xu N, Berenjian S, Berkhout B, et al. (2005) Suppression of RNA interference by adenovirus virus-associated RNA. J Virol 79: 9556–9565.
37. Subramanian T, Zhao LJ, Chinnadurai G (2013) Interaction of CtBP with adenovirus E1A suppresses immortalization of primary epithelial cells and enhances virus replication during productive infection. Virology 443: 313–320.
38. Boyd JM, Subramanian T, Schaeper U, La Regina M, Bayley S, et al. (1993) A region in the C-terminus of adenovirus 2/5 E1a protein is required for association with a cellular phosphoprotein and important for the negative modulation of T24-ras mediated transformation, tumorigenesis and metastasis. EMBO J 12: 469–478.
39. Chinnadurai G (2002) CtBP, an unconventional transcriptional corepressor in development and oncogenesis. Mol Cell 9: 213–224.
40. Yang J, Everett AD (2009) Hepatoma-derived growth factor represses SET and MYND domain containing 1 gene expression through interaction with C-terminal binding protein. J Mol Biol 386: 938–950.
41. Turner J, Crossley M (2001) The CtBP family: enigmatic and enzymatic transcriptional co-repressors. Bioessays 23: 683–690.
42. Nakai M, Komiya K, Murata M, Kimura T, Kanaoka M, et al. (2007) Expression of pIX gene induced by transgene promoter: possible cause of host immune response in first-generation adenoviral vectors. Hum Gene Ther 18: 925–936.

Published online: March 25, 2014

Scientific Report

SOURCE DATA TRANSPARENT PROCESS

EMBO reports

Structural determinants in GABARAP required for the selective binding and recruitment of ALFY to LC3B-positive structures

Alf Håkon Lystad[1], Yoshinobu Ichimura[2], Kenji Takagi[3], Yinjie Yang[2], Serhiy Pankiv[1], Yumi Kanegae[4], Shun Kageyama[2], Mariko Suzuki[4], Izumu Saito[4], Tsunehiro Mizushima[3], Masaaki Komatsu[2,**] & Anne Simonsen[1,*]

Abstract

Several autophagy proteins contain an LC3-interacting region (LIR) responsible for their interaction with Atg8 homolog proteins. Here, we show that ALFY binds selectively to LC3C and the GABARAPs through a LIR in its WD40 domain. Binding of ALFY to GABARAP is indispensable for its recruitment to LC3B-positive structures and, thus, for the clearance of certain p62 structures by autophagy. In addition, the crystal structure of the GABARAP-ALFY-LIR peptide complex identifies three conserved residues in the GABARAPs that are responsible for binding to ALFY. Interestingly, introduction of these residues in LC3B is sufficient to enable its interaction with ALFY, indicating that residues outside the LIR-binding hydrophobic pockets confer specificity to the interactions with Atg8 homolog proteins.

Keywords ALFY; GABARAP; LC3; LIR; structure
Subject Categories Autophagy & Cell Death; Membrane & Intracellular Transport; Structural Biology
DOI 10.1002/embr.201338003 | Received 24 September 2013 | Revised 21 February 2014 | Accepted 24 February 2014 | Published online 25 March 2014
EMBO Reports (2014) 15: 557–565

Introduction

Sequestration of cytoplasmic cargo for degradation by macroautophagy (hereafter autophagy) is facilitated by binding of cargo-interacting proteins, so-called autophagy receptors, to Atg8-homolog proteins, which upon the induction of autophagy becomes covalently linked to phosphatidylethanolamine (PE) in the autophagic membrane [1]. Whereas yeast has a single *Atg8* gene, mammals have seven Atg8 homologs, which can be divided into two subfamilies: the LC3 family (including LC3A, LC3B, LC3B2 and LC3C) and the GABARAP family (including GABARAP, GABARAPL1 and GABARAPL2) [2]. The reason for such an expansion of this protein family in higher eukaryotes is unclear, but it coincides with the expansion of cargo-recognition proteins and is likely to provide specificity to cargo recruitment.

The currently known autophagy receptors include receptors for the recognition of bacteria, viral particles, mitochondria, peroxisomes, midbody remnants and protein aggregates [1]. They generally interact with two hydrophobic pockets in the Atg8 proteins through a linear motif called an LC3-interacting region (LIR), having the consensus sequence [W/F/Y]-x-x-[I/L/V][1]. Whereas some autophagy receptors seem to interact with all Atg8 proteins *in vitro*, others show selective binding to a few Atg8 family members. The structural determinants in Atg8 proteins responsible for such selectivity remain to be determined in most cases, but it was recently shown that the specific interaction of the autophagy receptor NDP52 with LC3C requires, in addition to its noncanonical LIR motif xLVV (termed a CLIR), interactions outside the CLIR-binding pocket [3].

ALFY (autophagy-linked FYVE protein, also called WDFY3) is a large phosphatidyl-inositol 3-phosphate-binding protein shown to be recruited to ubiquitin-positive structures during stress. ALFY interacts with the ubiquitin-binding autophagy receptors p62/SQSTM1 and NBR1 [4,5] and contributes to autophagic clearance of aggregated proteins [5]. In this study, we show that ALFY binds selectively to the GABARAP subfamily, and weakly to LC3C, through a conserved LIR motif in its WD40 region. We demonstrate that the interaction of ALFY with GABARAPs is indispensable for the recruitment of LC3B to ALFY-p62-positive structures. We further identify three conserved residues in the GABARAPs that confer selectivity to the interaction with ALFY and show that introduction of these residues in the corresponding positions of LC3B is sufficient to enable interaction of ALFY with LC3B.

1 Institute of Basic Medical Sciences, University of Oslo, Oslo, Norway
2 Protein Metabolism Project, Tokyo Metropolitan Institute of Medical Science, Tokyo, Japan
3 Picobiology Institute, Graduate School of Life Science, University of Hyogo, Hyogo, Japan
4 Laboratory of Molecular Genetics, Institute of Medical Science, University of Tokyo, Tokyo, Japan
*Corresponding author. Tel: +47 22851110; Fax: +47 22851058; E-mail: anne.simonsen@medisin.uio.no
**Corresponding author. Tel: +81 3 5316 3244; Fax: +81 3 5316 3152; E-mail: komatsu-ms@igakuken.or.jp

Published online: March 25, 2014
EMBO reports

Results and Discussion

ALFY interacts selectively and directly with LC3C and GABARAP family proteins

ALFY was identified in a proteomic approach aimed at finding new GABARAP-interacting proteins (Unpublished observations). In order to verify this interaction, cells were transfected with GFP-tagged Atg8 homologs of the LC3 and GABARAP subfamilies, followed by anti-GFP immunoprecipitation (IP) and immunoblotting for endogenous ALFY (Fig 1A). Whereas there was little or no interaction between ALFY and LC3A or LC3B, ALFY was found to co-IP with GABARAP, GABARAPL1 and GABARAPL2, but also weakly with LC3C (Fig 1A).

To determine the minimal region of ALFY required for its interaction with GABARAP, we initially performed GST pull-down assays with *in vitro*-translated GFP-ALFY constructs that covered its entire cDNA sequence (Fig 1B). The C-terminal part of ALFY was found to interact strongly with GABARAP, and the binding site was mapped to amino acid (aa) 3313–3363, located between the fourth and fifth WD40 repeat of ALFY (Fig 1B, C). This part of ALFY was also sufficient to co-IP endogenous GABARAP when transfected into HEK293T cells (Supplementary Fig S1A, B). The interaction between ALFY and GABARAPs was shown to be direct, as recombinant ALFY (aa 2981–3526) was efficiently pulled down with GST-GABARAPs and weakly with GST-LC3C (Fig 1D). These results indicate that ALFY selectively and directly interacts with LC3C and GABARAP family proteins.

Identification of a LIR in ALFY

When aligning the $ALFY_{3313–3363}$ sequence with the LIR consensus motif [W/F/Y]-x-x-[I/L/V], we found one perfect alignment, F-I-F-V (aa 3346–3349), that was conserved in homologous ALFY sequences (Fig 2A). Mutation of the potential LIR residues F3346, I3347, F3348 or V3349 to Ala/A all caused a large decrease in the binding of *in vitro*-translated GFP-$ALFY_{2981–3526}$ to GABARAP and LC3C (Fig 2B and Supplementary Fig S1C). As the first Phe/F of the core LIR proved essential for the interactions, we propose that binding of ALFY to Atg8 homolog proteins is mediated by a canonical LIR motif. However, as mutation of the I3347 residue had a greater impact on the binding to LC3C than to GABARAP, we cannot exclude the possibility that ALFY has a hybrid LIR/CLIR motif. The importance of this motif was further validated with purified proteins, showing that MBP-$ALFY_{3255–3526}$, but not the LIR mutant ($ALFY_{3255–3526\ F3346A}$), was able to interact directly with GABARAP (Fig 2C). To further investigate the affinity of ALFY for different Atg8 proteins, we performed isothermal titration calorimetry (ITC) (Fig 2D and Supplementary Fig S1D). The ALFY-LIR peptide (aa 3341–3354) used in this assay showed similar binding specificity for Atg8 proteins, with strong affinity to the GABARAP family proteins (0.327–0.871 μM), weak affinity for LC3C (20.8 μM) and no interaction with LC3B. Furthermore, we show that the LIR motif is functionally conserved, as the corresponding LIR peptide from the *Drosophila* ALFY homolog, Blue Cheese [6], bound strongly and specific to purified dAtg8a protein (Fig 2E), in line with dAtg8a being more similar to GABARAPs than LC3s.

Overall structure of the GABARAP-ALFY-LIR complex

Next we decided to determine the structure of the GABARAP-ALFY-LIR complex (PDB ID code 3WIM) by X-ray crystallography (Fig 3A and Supplementary Table S1). The complex consists of full-length GABARAP (aa 1–117) bound to an ALFY-LIR peptide (aa 3341–3354), and its crystal structure was determined by molecular replacement using wild-type GABARAP (PDB ID code 1GNU) and refined to 2.6 Å resolution (Fig. 3A). This represents the first structural determination of GABARAP with a physiological LIR-containing peptide and is essentially identical to the previously reported structures of peptide-free GABARAP [7,8]. The ALFY-LIR-binding surface of GABARAP consists of three linkers (α2-β1, β1-β2 and β2-α3), an α-helix (α2) and two β-strands (β1 and β2). The side chains of the core ALFY-LIR residues (F3346 and V3349) are bound deeply into two hydrophobic pockets of GABARAP (Supplementary Fig S2A and B), similar to that observed between LC3B and the LIR moiety of other LIR-containing proteins, including p62 [9], Atg4B [10] and optineurin [11].

Conserved residues in GABARAP determine the binding specificity of ALFY

To try to understand why ALFY interacts with GABARAP and not with LC3B, we superimposed the LC3B structure (PDB ID code 1UGM) onto the GABARAP-ALFY-LIR structure (Fig 3B). While both LC3B and GABARAP can accommodate the core ALFY-LIR residues (F3346 and V3349), it is clear from this model that D3344 of the ALFY-LIR is able to form ionic interactions with K24 and Y25 of GABARAP, but not with the corresponding Q26 and H27 of LC3B (Fig 3B and Supplementary Fig S2C). Moreover, while D54 of GABARAP can interact with Y3351 of the ALFY-LIR, the corresponding H57 of LC3B causes steric hindrance between the two side chains (Fig 3B and Supplementary Fig S2D). Interestingly, the

Figure 1. The C-terminal region of ALFY interacts with GABARAP.

A Transfected GFP-Atg8 homologs were immunoprecipitated with μMACSTM from total U2OS cell extracts followed by immunoblot analysis with anti-GFP and anti-ALFY antibodies. Data are representative of two independent experiments.

B An overview of the deletion mutant constructs of ALFY used for GST pull-down experiments in (C).

C The indicated ^{35}S-labelled *in vitro*-translated GFP-tagged constructs were incubated with GST, GST-LC3B or GST-GABARAP conjugated to glutathione Sepharose, and their binding was evaluated by autoradiography (ARG). 5% of the *in vitro*-translated protein (arrow head) used was loaded. Equal amounts of GST proteins were used as shown by Coomassie Brilliant Blue (CBB) staining. Data are representative of three independent experiments.

D Recombinant ALFY (aa 2981–3526) was incubated with GST-Atg8 proteins conjugated to glutathione Sepharose. The pulled-down complexes were subjected to SDS–PAGE and anti-ALFY and anti-GST immunoblotting. 5% of the recombinant ALFY protein used was loaded as input. Data are representative of three independent experiments.

Source data are available online for this figure.

Published online: March 25, 2014

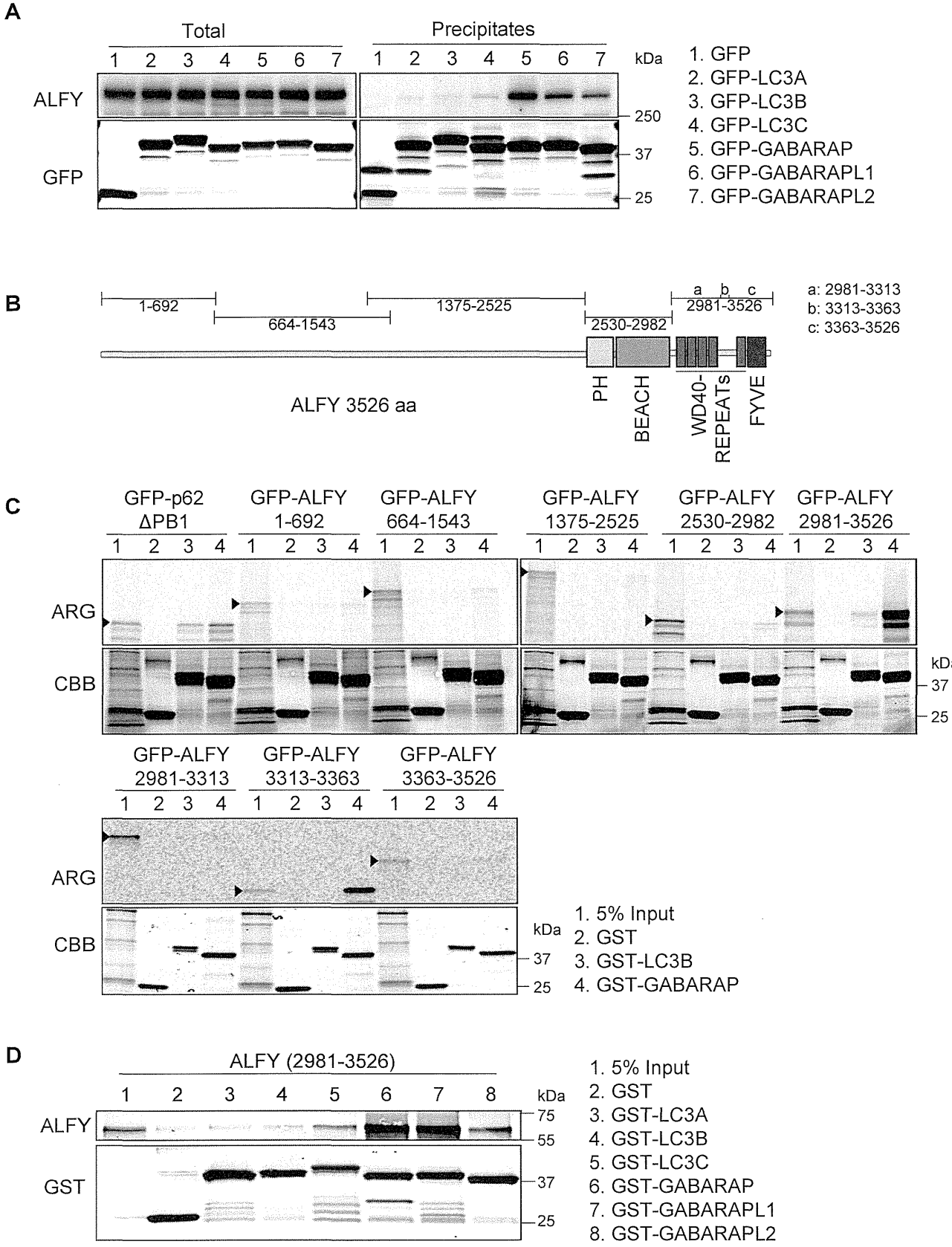

Published online: March 25, 2014
EMBO reports

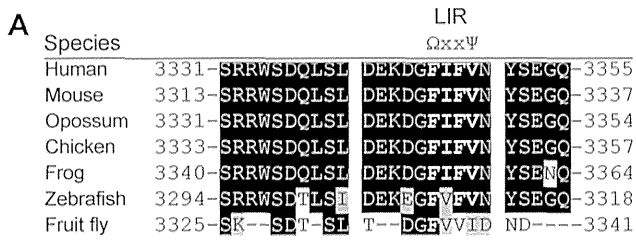

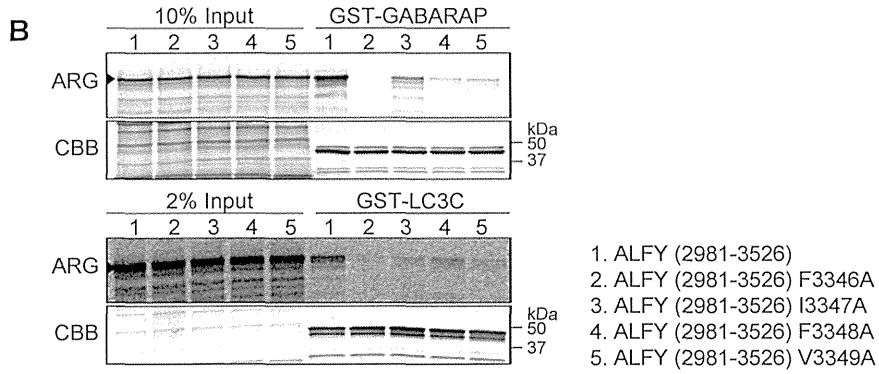

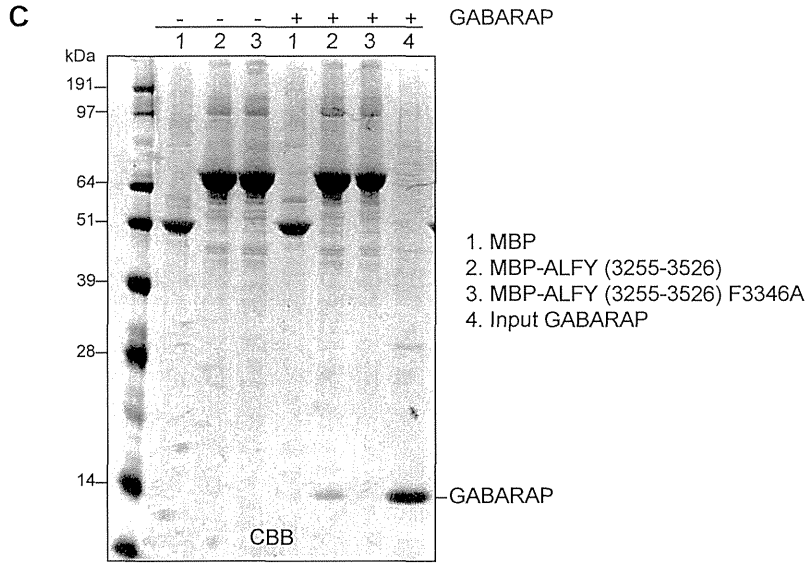

D

PROTEIN	LC3B	LC3C	GABARAP	GABARAPL1	GABARAPL2
K_D (μM)	ND	20.8±3.16	0.327±0.03	0.387±0.021	0.871±0.119
N (sites)	ND	0.87±0.04	0.956±0.003	0.921±0.002	1.06±0.007
ΔH (cal mol^{-1})	ND	-4940±340.9	-7456±45.28	-6818±20.78	-5710±64.15
ΔS (cal mol^{-1} deg^{-1})	ND	4.90	4.69	6.47	8.61

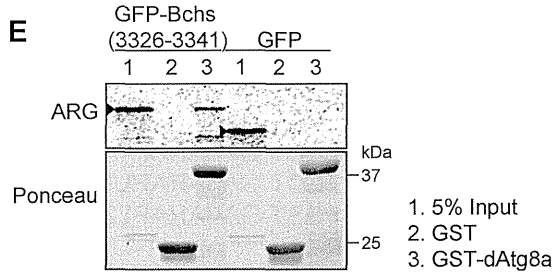

Published online: March 25, 2014

Figure 2. Identification of the LC3-interacting region (LIR) in ALFY.

A Alignment of the potential LIR in human ALFY to the corresponding homolog sequences of representatives of mammals, birds, fish and insects. Ω indicates an aromatic residue, while Ψ indicates an aliphatic residue.

B ^{35}S-labelled *in vitro*-translated GFP-ALFY (aa 2981–3526) wild-type and different LIR mutants were incubated with GST-GABARAP or -LC3C and binding evaluated by ARG. 10 and 2% of the *in vitro*-translated proteins used were loaded to illustrate binding affinity. CBB staining shows equal amounts of GST proteins used. Data are representative of three independent experiments.

C MBP, MBP-ALFY (aa 3255–3526) or the ALFY-LIR mutant (F3346A) conjugated to amylose resins was incubated in the absence or presence of purified GABARAP. The pulled-down complexes were subjected to SDS–PAGE and visualized by CBB staining. Data are representative of three independent experiments.

D Thermodynamic parameters of ALFY-LIR peptide (aa 3341–3354) to Atg8 homologs. All titrations were performed at 25°C as described in Supplementary Methods. ITC data were fitted to a one-site binding model. ND, not detected.

E ^{35}S-labelled *in vitro*-translated GFP or GFP-Bchs (aa 3326–3341) were incubated with GST or GST-dAtg8a and binding evaluated by ARG. 5% of the *in vitro*-translated protein used was loaded. Ponceau staining shows equal amounts of GST proteins used. Data are representative of three independent experiments.

Source data are available online for this figure.

K24/Y25/D54 residues of GABARAP are conserved in GABARAPL1 and GABARAPL2 (Fig 3C), which both bind to ALFY (Figs 1A, D and 2D). Moreover, the corresponding residues in LC3C (K32/F33/E63) are similar to the GABARAP subfamily (Fig 3C) and have been implicated in the specific binding to NDP52 [3]. We therefore speculated that these three residues are responsible for the specific interaction of ALFY with GABARAPs and LC3C. In order to test this experimentally, we substituted these three amino acids in LC3B with the corresponding amino acids of GABARAP and created HeLa cells with stable inducible expression of the triple mutant protein (GFP-LC3B Q26K/H27Y/H57D). When compared to cells expressing wild-type LC3B, we found increased binding of endogenous ALFY to the LC3B triple mutant (Q26K/H27Y/H57D) (Fig 3D). We next substituted these three residues in GABARAP with the corresponding LC3B residues, either individually or combined (Fig 3E, F). While the GABARAP single mutants had little or no effect on the interaction with ALFY, the triple GABARAP mutant (K24Q/Y25H/D54H) was significantly compromised in the ability to bind to MBP-ALFY$_{3255–3526}$ (Fig 3E, F and Supplementary Fig S2E). Moreover, in line with our result in Fig 3D, recombinant protein of the LC3B triple mutant (Q26K/H27Y/H57D) showed a strong and LIR-dependent interaction with MBP-ALFY$_{3255–3526}$ (Fig 3F). In contrast, the interaction between p62 and GABARAP/LC3B proteins was not affected to the same degree by mutation of these residues, as both the LC3B triple mutant (Q26K/H27Y/H57D) and the GABARAP triple mutant (K24Q/Y25H/D54H) bound to MBP-p62$_{168–391}$ with similar affinity as to wild-type GABARAP/LC3B proteins (Fig 3F). To test whether the ALFY-LIR residues involved in interactions with GABARAP K24/Y25/D54 were equally required for the specificity of the interaction, these residues (K3343/D3344/Y3351) were mutated in GFP-ALFY$_{2981–3526}$. As can be seen in Fig 3G, the interaction with GABARAP was drastically reduced, whereas no increased affinity towards LC3B was detected, indicating that these ALFY residues provide selective binding to GABARAP, rather than block the interaction with LC3B. Taken together, we conclude that while the core LIR residues of ALFY are essential for its interaction with GABARAP, additional residues outside the core LIR motif confer specificity to the interaction of ALFY with GABARAP.

GABARAP is required for recruitment of LC3B to ALFY-positive structures and for the clearance of ALFY-p62-positive bodies

We have previously found that ALFY is recruited to cytoplasmic Ub- and p62-positive bodies upon stress such as amino acid starvation, proteasomal inhibition and puromycin treatment [4,12]. We here show that endogenous LC3B (Supplementary Fig S3), as well as stably expressed GFP-GABARAP (Fig 4A), colocalized with endogenous ALFY in stress-induced cytoplasmic structures. Interestingly, full-length wild-type GFP-ALFY, but not the LIR mutant, was recruited to GABARAP and LC3B-positive structures when expressed in ALFY-deficient MEFs (Fig 4B and Supplementary Fig S4). As ALFY does not interact with LC3B, and has very low affinity for LC3C, which is not present in mice and expressed at very low levels in HeLa and Hek293 cells (Unpublished data and Supplementary Fig S5A), we conclude that interaction of ALFY with GABARAP is required for its colocalization with LC3B. In line with this, while overexpressed ALFY$_{2285–3526}$ did not colocalize with wild-type GFP-LC3B, colocalization was observed upon the induction of excess GABARAP (Supplementary Fig S5B) or expression of the GFP-LC3B (Q26K/H27Y/H57D) mutant (Supplementary Fig S5B), indicating that the structural determinants identified as being important for GABARAP-ALFY binding specificity also determine colocalization between these proteins. GFP-GABARAP, -LC3B and -LC3B (Q26K/H27Y/H57D) stably expressed in these cell lines were considered functional as they retained the ability to become lipidated (Supplementary Fig S6A).

Further supporting a role of GABARAP in recruiting LC3B-positive membranes to ALFY-positive structures, we found an accumulation of ALFY-p62-positive structures that were negative for LC3B in GABARAP-depleted cells, whereas ALFY-p62-LC3B-positive structures were seen in control cells (Fig 4C). Interestingly, p62- and LC3B-positive puncta lacking ALFY could be detected in siGABARAP cells (Fig. 4C). Thus, our data indicate that a subset of p62-positive structures localizes with LC3B in the absence of GABARAP, but that recruitment of LC3B to ALFY-p62 positive bodies, or *vice versa*, requires GABARAP. We have previously found that ALFY is required for packing of p62 oligomers into larger p62 bodies, as well as for their clearance by autophagy [4]. Consistent with this, the accumulation of Triton X-100-insoluble p62 seen in cells where autophagic flux was inhibited by bafilomycin A1 was prevented both in ALFY-depleted HeLa cells (Fig 4D) and in ALFY KO MEFs (Fig 4E). Taken together, our results argue that the ALFY-GABARAP interaction is important for targeting of certain p62 structures for clearance by autophagy (Fig 4F). In line with our previous data [5], depletion of ALFY did neither affect the total level, the lipidation nor the turnover of Atg8 proteins (LC3B, GABARAP and GABARAPL1) in response to starvation (Supplementary Fig S6B).

Published online: March 25, 2014
EMBO reports

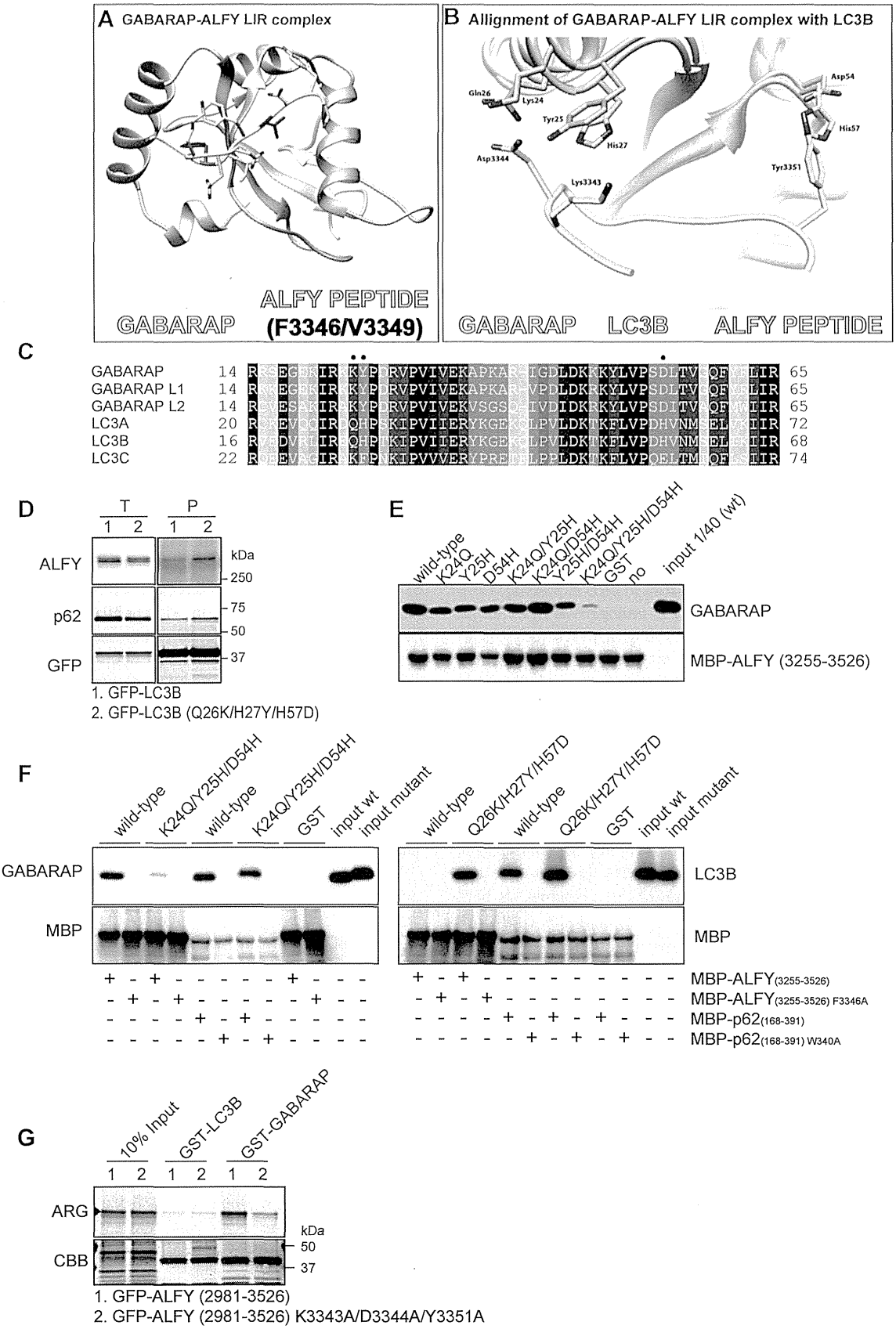

Published online: March 25, 2014

Figure 3. Structural analysis of GABARAP-ALFY peptide complex.

A Overall structure of the complex formed by GABARAP in brown and the ALFY-LIR peptide in yellow with the core LC3-interacting region (LIR) motif highlighted in dark blue.

B Alignment of the GABARAP-ALFY-LIR peptide complex structure with the published structure of LC3B (1UGM), using UCSF Chimera. See Supplementary Fig S2C and D for calculation of the distances between the residues highlighted as sticks in the ALFY-LIR peptide and the corresponding annotated residues in GABARAP or LC3B.

C Sequence alignment of human Atg8 protein homologs. The alignment was obtained by Clustal W. Black and grey backgrounds represent degree of similarity. Closed circles indicate specific residues of GABARAP involved in the ALFY-LIR peptide interaction.

D GFP-LC3B and GFP-LC3B (Q26K/H27Y/H57D) were immunoprecipitated with GFP-TRAP® from total cell lysate of stably transfected HeLa FlpIn cells, followed by SDS–PAGE and immunoblotting with the indicated antibodies. Data are representative of three independent experiments.

E MBP-ALFY$_{3255–3526}$ conjugated to amylose resin was incubated with GST or the indicated GABARAP mutants. The pulled-down complexes were subjected to SDS–PAGE and visualized by immunoblotting with anti-MBP and anti-GABARAP antibodies. Data are representative of three independent experiments.

F MBP-tagged ALFY$_{3255–3526}$ and p62$_{168–391}$ or their corresponding LIR mutants (F3346A and W340A, respectively) were conjugated to amylose resin and incubated with purified GST, GABARAP, GABARAP mutant (K24Q/Y25H/D54H), LC3B or LC3B mutant (Q26K/H27Y/H57D). The bound proteins were visualized by immunoblotting with anti-GABARAP, anti-LC3 and anti-MBP antibodies. Data are representative of three independent experiments.

G ^{35}S-labelled *in vitro*-translated GFP-ALFY (aa 2981–3526) wild-type and K3343A/D3344A/Y3351A mutant were incubated with GST-LC3B and GABARAP and binding evaluated by ARG. 10% of the *in vitro*-translated proteins used was loaded. CBB staining shows equal amounts of GST proteins used. Data are representative of three independent experiments.

Source data are available online for this figure.

Although the precise function of the different Atg8 homologs largely remains to be characterized, they have all been implicated in autophagy, either by recruiting cargo through their interaction with autophagy receptor proteins or by facilitating different steps of autophagosome biogenesis [2]. However, many open questions remain to be addressed, as whether LC3/GABARAP proteins act by recruiting different types of cargo or cooperate in cargo recruitment by binding different cargo-bound autophagy receptors, or whether they function sequentially in the pathway or in response to various types of stimuli.

In contrast, an extensive effort over the past few years has led to the identification of several LC3/GABARAP-interacting proteins, determination of LIR/CLIR motifs and functional characterization of many such proteins. It seems clear that while cargo-recruiting autophagy receptors (e.g. p62, NBR1 and optineurin) are specifically recruited to the inner surface of the phagophore and themselves become degraded by autophagy [13–15], other proteins (e.g. Rab effectors) associate in a LIR-dependent manner to the outer surface of the autophagosomes to facilitate their transport [16–18]. A third group of Atg8-interacting proteins (e.g. ULK1 complex proteins) [19] seems to be involved in scaffolding of protein complexes to allow their interaction with the phagophore membrane, without being themselves degraded by autophagy. We speculate that ALFY belongs to the latter group, as it is required for the recruitment of core Atg proteins to p62-positive protein aggregates, without becoming degraded by autophagy itself (Fig 4F) [4,5]. Interestingly, similar to ALFY, ULK1 complex proteins were found to interact preferentially with GABARAPs through FxxV/I LIR motifs, and their LIR-dependent interactions with GABARAP seem to facilitate their recruitment to LC3B-positive structures [19]. How and when these Atg8-interacting proteins are eventually released from the forming autophagosome is not known, but a regulation of their interaction with GABARAP is likely involved.

Materials and Methods

The experimental procedures, as well as plasmids used (Supplementary Table S2), are described in detail in the supplementary information online.

Cell culture

HeLa, U2OS and MEFs were used for transfection of constructs or siRNA. FlpIn T-Rex™ HeLa cells with stable inducible expression of GFP-GABARAP or GFP-LC3B were induced with 500 ng/ml tetracycline for 24 h.

Immunofluorescence microscopy

Confocal images were acquired on an Olympus FluoView 1000 confocal laser-scanning microscope. Image processing and analysis

Figure 4. Physiological role of the interaction between ALFY and GABARAP.

A HeLa FlpIn GFP-GABARAP cells were treated with proteasomal inhibitor (MG132, 2 h) or subjected to amino acid starvation (EBSS, 2 h), before staining with anti-ALFY antibodies. Scale bar, 10 μm.

B GFP-tagged full-length ALFY wild-type or LC3-interacting region (LIR)-mutant was expressed into *Alfy*-deficient MEFs using an adenovirus system. At 48 h after infection, the MEFs were cultured in normal media or EBSS for 1.5 h before staining with anti-LC3B or anti-GABARAP antibodies. Scale bars 10 μm.

C HeLa cells were treated with control or siRNA targeting GABARAP, GABARAPL1 and GABARAPL2. 72 h after transfection cells were immunostained with anti-LC3B, anti-ALFY and anti-p62 antibodies. Scale bars, 10 μm.

D HeLa cells were treated with control or siRNA targeting ALFY. 72 h after transfection, cells were treated with puromycin with or without bafilomycin A1 for 2 h and total cell lysates were fractionated into TX-100-soluble and insoluble fractions. The TX-100-soluble/insoluble fractions were then immunoblotted with the indicated antibodies. Data are representative of three independent experiments.

E ALFY WT and KO MEFs were treated with puromycin or EBSS with or without bafilomycin A1 for 2 h and the total cell lysates were then fractionated into Triton X-100 (TX-100)-soluble and insoluble fractions. The TX-100-soluble/insoluble fractions were then immunoblotted with the indicated antibodies. Data are representative of three independent experiments.

F Schematic model of ALFY-mediated selective autophagy.

Source data are available online for this figure.

Published online: March 25, 2014
EMBO reports

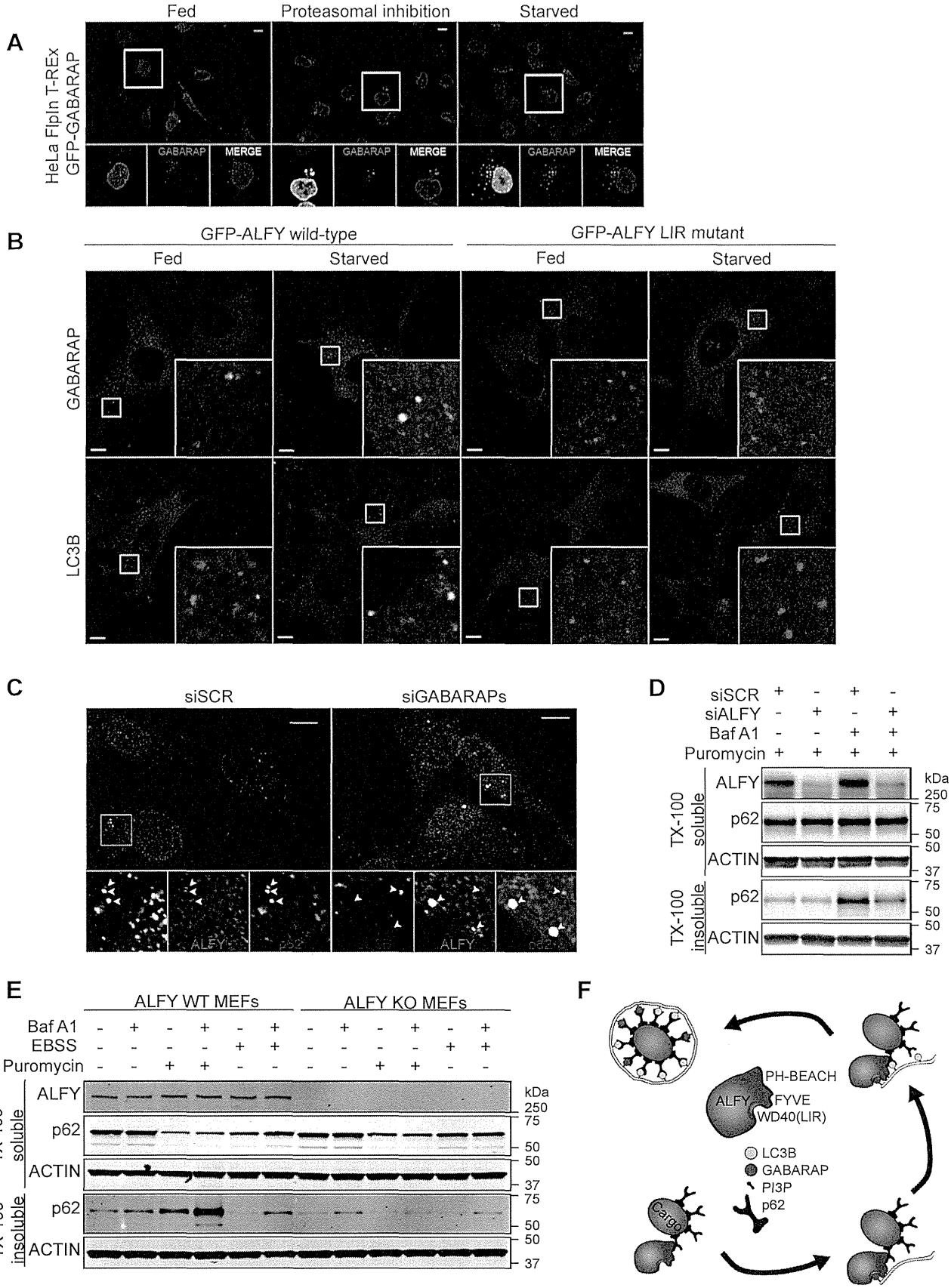

were done with OLYMPUS FLUOVIEW Viewer software and Adobe Photoshop CS4 (Adobe Systems).

In vitro pull-down assays

GFP- and STREP-FLAG-tagged proteins were pulled down using GFP-TRAP, μMACS (Miltenyi Biotec) or Strep-Tactin Sepharose (IBA). ^{35}S-methionine-labelled *in vitro*-translated GFP-tagged proteins were mixed with GST-tagged Atg8 proteins bound to glutathione Sepharose (GE Healthcare Bio-Sciences). For direct binding assays, MBP-tagged proteins were pulled down with GST-tagged proteins. Alternatively, precision protease was used to cleave off the GST tag before their incubation with recombinant MBP proteins and precipitation with amylose resin (New England Biolabs).

Crystal structure

The crystal structure of the GABARAP-ALFY peptide complex (PDB ID code 3WIM) was solved by molecular replacement using the structure of wild-type GABARAP (PDB ID code 1GNU) as the search model.

Supplementary information for this article is available online: http://embor.embopress.org

Acknowledgements

We thank T. Mita (Tokyo Metropolitan Institute of Medical Science) for his help with cell biological and biochemical studies, A. Kunida (University of Tokyo) for digital PCR analysis and all members of beamline BL44XU for help in data collection at SPring-8. This work was supported by grants from the Research Council of Norway and the Norwegian Cancer Society (to AS) and from a Grant-in-Aid for Scientific Research on Innovative Areas (to MK).

Author contributions

AHL, SP, MK and AS designed the experiments; AHL, YI, YY, SK and SP carried out the biochemical and cell biological experiments; KT, TM and AS completed the structural analysis; YK, MS and IS made the adenovirus vectors; AHL, SP and AS analysed the data; AHL, TM, MK and AS wrote the manuscript. All authors discussed the results and commented on the manuscript.

Conflict of interest

The authors declare that they have no conflict of interest.

References

1. Johansen T, Lamark T (2011) Selective autophagy mediated by autophagic adapter proteins. *Autophagy* 7: 279–296
2. Shpilka T, Weidberg H, Pietrokovski S, Elazar Z (2011) Atg8: an autophagy-related ubiquitin-like protein family. *Genome Biol* 12: 226
3. von Muhlinen N, Akutsu M, Ravenhill BJ, Foeglein A, Bloor S, Rutherford TJ, Freund SM, Komander D, Randow F (2012) LC3C, bound selectively by a noncanonical LIR motif in NDP52, is required for antibacterial autophagy. *Mol Cell* 48: 329–342
4. Clausen TH, Lamark T, Isakson P, Finley K, Larsen KB, Brech A, Overvatn A, Stenmark H, Bjorkoy G, Simonsen A et al (2010) p62/SQSTM1 and ALFY interact to facilitate the formation of p62 bodies/ALIS and their degradation by autophagy. *Autophagy* 6: 330–344
5. Filimonenko M, Isakson P, Finley KD, Anderson M, Jeong H, Melia TJ, Bartlett BJ, Myers KM, Birkeland HC, Lamark T et al (2010) The selective macroautophagic degradation of aggregated proteins requires the PI3P-binding protein Alfy. *Mol Cell* 38: 265–279
6. Finley KD, Edeen PT, Cumming RC, Mardahl-Dumesnil MD, Taylor BJ, Rodriguez MH, Hwang CE, Benedetti M, McKeown M (2003) blue cheese mutations define a novel, conserved gene involved in progressive neural degeneration. *J Neurosci* 23: 1254–1264
7. Knight D, Harris R, McAlister MS, Phelan JP, Geddes S, Moss SJ, Driscoll PC, Keep NH (2002) The X-ray crystal structure and putative ligand-derived peptide binding properties of gamma-aminobutyric acid receptor type A receptor-associated protein. *J Biol Chem* 277: 5556–5561
8. Stangler T, Mayr LM, Willbold D (2002) Solution structure of human GABA(A) receptor-associated protein GABARAP: implications for biological function and its regulation. *J Biol Chem* 277: 13363–13366
9. Ichimura Y, Kumanomidou T, Sou YS, Mizushima T, Ezaki J, Ueno T, Kominami E, Yamane T, Tanaka K, Komatsu M (2008) Structural basis for sorting mechanism of p62 in selective autophagy. *J Biol Chem* 283: 22847–22857
10. Satoo K, Noda NN, Kumeta H, Fujioka Y, Mizushima N, Ohsumi Y, Inagaki F (2009) The structure of Atg4B-LC3 complex reveals the mechanism of LC3 processing and delipidation during autophagy. *EMBO J* 28: 1341–1350
11. Rogov VV, Suzuki H, Fiskin E, Wild P, Kniss A, Rozenknop A, Kato R, Kawasaki M, McEwan DG, Lohr F et al (2013) Structural basis for phosphorylation-triggered autophagic clearance of Salmonella. *Biochem J* 454: 459–466.
12. Simonsen A, Birkeland HC, Gillooly DJ, Mizushima N, Kuma A, Yoshimori T, Slagsvold T, Brech A, Stenmark H (2004) Alfy, a novel FYVE-domain-containing protein associated with protein granules and autophagic membranes. *J Cell Sci* 117: 4239–4251
13. Pankiv S, Clausen TH, Lamark T, Brech A, Bruun JA, Outzen H, Overvatn A, Bjorkoy G, Johansen T (2007) p62/SQSTM1 Binds Directly to Atg8/LC3 to facilitate degradation of ubiquitinated protein aggregates by autophagy. *J Biol Chem* 282: 24131–24145
14. Kirkin V, Lamark T, Sou YS, Bjorkoy G, Nunn JL, Bruun JA, Shvets E, McEwan DG, Clausen TH, Wild P et al (2009) A role for NBR1 in autophagosomal degradation of ubiquitinated substrates. *Mol Cell* 33: 505–516
15. Wild P, Farhan H, McEwan DG, Wagner S, Rogov VV, Brady NR, Richter B, Korac J, Waidmann O, Choudhary C et al (2011) Phosphorylation of the autophagy receptor optineurin restricts Salmonella growth. *Science* 333: 228–233
16. Pankiv S, Alemu EA, Brech A, Bruun JA, Lamark T, Overvatn A, Bjorkoy G, Johansen T (2010) FYCO1 is a Rab7 effector that binds to LC3 and PI3P to mediate microtubule plus end-directed vesicle transport. *J Cell Biol* 188: 253–269
17. Itoh T, Kanno E, Uemura T, Waguri S, Fukuda M (2011) OATL1, a novel autophagosome-resident Rab33B-GAP, regulates autophagosomal maturation. *J Cell Biol* 192: 839–853
18. Popovic D, Akutsu M, Novak I, Harper JW, Behrends C, Dikic I (2012) Rab GTPase-activating proteins in autophagy: regulation of endocytic and autophagy pathways by direct binding to human ATG8 modifiers. *Mol Cell Biol* 32: 1733–1744
19. Alemu EA, Lamark T, Torgersen KM, Birgisdottir AB, Larsen KB, Jain A, Olsvik H, Overvatn A, Kirkin V, Johansen T (2012) ATG8 family proteins act as scaffolds for assembly of the ULK complex: sequence requirements for LC3-interacting region (LIR) motifs. *J Biol Chem* 287: 39275–39290